Student thesis series INES nr 574

Mapping wetlands in Sweden using multi-source satellite data and random forest algorithm

Salvador Antonio Hernández Malavé

2022
Department of
Physical Geography and Ecosystem Science
Lund University
Sölvegatan 12
S-223 62 Lund
Sweden

Salvador Antonio Hernández Malavé (2022).

Mapping wetlands in Sweden using multi-source satellite data and random forest algorithm

Master's degree thesis, 30 credits in Subject of Degree

Department of Physical Geography and Ecosystem Science, Lund University

Level: Master of Science (MSc)

Course Duration: January 2022 – June 2022

Mapping wetlands in Sweden using multi-source satellite data and Random Forest algorithm

---

Salvador Antonio Hernández Malavé

Master thesis, 30 credits, in *Geomatics*

Supervisor:
Zheng Duan
Dep. of Physical Geography and Ecosystem Science, Lund University

Examiner:
Thomas Pugh
Dep. of Physical Geography and Ecosystem Science, Lund University

Table of Contents

Table of Figures

Index of Tables

Mapping wetlands in Sweden using multi-source satellite data and Random Forest algorithm

Wetlands are valuable ecosystems, and assets for human life, that must be regularly monitored, starting with accurately mapping their location and extent. However, an updated national inventory of wetlands is needed. The availability of multi-source data, and advanced machine learning algorithms in Google Earth Engine (GEE) offers excellent opportunities to map wetlands on a country-wide scale. This study mapped wetlands in Sweden using optical, radar, and topographical data, with the Random Forest algorithm, and labels from digitized polygons within the boundaries of the latest national wetlands inventory of Sweden (VMI), completed in 2005. This study discriminates between three classes (non-wetlands, wetlands, and water). From the digitized polygons, 30,000 points were sampled per class in each county (1,890,000 in total). A single RF classifier was trained for each county of Sweden, and a new Swedish national wetlands inventory (RFWI) was generated. The accuracy assessment with testing samples showed that the country-wide overall accuracy (OA) of the classified validation set of points is 98.97%, with a kappa value of 0.985, where the counties with the best, and worst OA are Kronoberg (99.84%), and Norrbotten (97.40%), respectively. RFWI agrees with VMI to a large extent, thus, there are new wetlands mapped, and wetlands surveyed in VMI disappeared. The countrywide area classified as wetlands in RFWI is 30.8% bigger than VMI, as VMI does not incorporate many small wetlands. Nevertheless, the results between counties are mixed. Six out of the 21 counties are estimated to have suffered an overall loss of wetlands area, as big as 73%. RFWI wetlands coverage is higher than VMI's in the remaining counties, lesser than 30% (small) in seven counties, between 38-64% (mild) in four, between 202-245% (high) in other three, while Stockholm presents a huge difference (450%). The decrease observed in some counties was corroborated with Google Earth imagery. The small, and mild differences are due to the incorporation of wetlands not present in VMI. While high, and huge differences found in four counties are overestimated due to label-related issues. Approximately 70% of the areal difference between RFWI & VMI is contained in Jämtland county. Besides VMI, the developed RFWI was compared to other continental, and global wetlands products specifically LUCAS, ESA WorldCover, the Ramsar Database, MODIS LC1, and GLWD-3. LUCAS dataset was reclassified to match this study's classes, and for extracting the class from RFWI, this procedure indicated good agreement between the products (87.88% OA). All the other large-scale inventories mentioned underestimated wetlands occurrence in Sweden to a large extent. The area of wetlands in RFWI could be considered as a realistic maximum in most counties except Stockholm, and Jämtland. Limitations of this study are discussed and recommendations for future studies are given.

Keywords: physical geography and ecosystem analysis, multi-temporal, google earth engine, GEE, machine learning, classification, country-wide

Advisor: **Zheng Duan**.

Master degree project 30 credits in Geomatics, 2022. Dep. of Physical Geography and Ecosystem Science, Lund University. Student thesis series INES nr 574

List of abbreviations

ARD	Analysis Ready Data
BOA	Bottom of Atmosphere
DEM	Digital Elevation Model
EO	Earth Observation
GEE	Google Earth Engine
ha	hectare
IR	InfraRed
LC	Land Cover
LM1	Labeling Method 1
LM2	Labeling Method 2
LUCAS	Land Use and Coverage Area frame Survey
ML	Machine Learning
MODIS	Moderate Resolution Imaging Spectroradiometer
NDVI	Normalized Difference Vegetation Index
NDWI	Normalized Difference Water Index
NIR	Near InfraRed (Electromagnetic Spectrum)
OA	Overall Accuracy
RFWI	Random Forest Wetlands Inventory
RS	Remote Sensing
SAR	Synthetic Aperture Radar
SD	Standard Deviation
SWIR	Short-wave InfraRed
S1	Sentinel-1 Satellite
S2	Sentinel-2 Satellite
TOA	Top of Atmosphere
TPI	Topological Position Index
TWI	Topological Wetness Index
VH	Vertical transmit Horizontal receive radar polarization
VIS	Visible (Electromagnetic Spectrum)
VMI	Wetlands Inventory (Våtmarksinventeringen)
VV	Vertical transmit Vertical receive radar polarization

1 Introduction

Wetlands are complex ecosystems that remain submerged in water for a great part of the year (Gunnarsson & Löfroth, 2009; Reddy & DeLaune, 2008; Zedler & Kercher, 2005). Wetlands are highly productive, very diverse, and providers of multiple ecosystem services, e.g. hazard protection, carbon sequestration, and water treatment, among others, valued in thousands of billions of US dollars globally (Zedler & Kercher, 2005). Regrettably, the number of wetlands, and their extent, have drastically diminished in the last 3 centuries, estimated to be today around 50-80% of what it was in 1700 (Davidson, 2014), mostly due to anthropogenic activities. But the lack of long-term maps, and the often poor or inexistent efforts made for mapping them, difficult the task of understanding how these ecosystems are changing (Davidson, 2014).

Global efforts have been made to generate wetlands Land Cover (LC) maps, and wetlands inventories using a wide range of methods. These methods can be generally divided into field surveys, aerial photograph interpretation, and satellite imagery classification. Global wetlands inventories and land cover datasets including wetlands have been produced, e.g. European Space Agency (ESA) WorldCover LC Product (Zanaga et al., 2021), The Ramsar Database (Ramsar Convention Secretariat, 2016), The Global Lake and Wetlands Database (Lehner & Döll, 2004), MODIS LC products (Friedl et al., 2010). However, the accuracies vary between countries and are limited in the coverage (a small number of wetlands are included in these datasets). Land Use and Coverage Area frame Survey (LUCAS) captures high-quality field samples in the European continent, including wetlands, but has a coarse resolution, and only a fraction of the sites were visited in the field. Thus, national, and local efforts provide better, and more detailed maps of wetlands.

The Swedish Environmental Protection Agency along with county-based agencies finished the National Wetlands Inventory (VMI) in 2005. It contains about 35,000 objects (wetlands), surveyed from visual interpretation of black and white aerial photographs. Most of those photographs were captured before 1986, with support from Infrared (IR) photographs in the 1986-2005 period (Gunnarsson & Löfroth, 2009). VMI has several limitations: (1) it underestimates the total wetlands area due to the following reasons. It only includes wetlands bigger than 10 hectares (ha) from Sweden's center to the southernmost region, and bigger than 50 ha in the northern region (Appendix A figure A.1.). Additionally, only wetlands in low elevations were considered, excluding wetlands from the alpine regions. (2) It is 15 years after the completion of VMI, and thus VMI could be potentially outdated, considering the changes in extents for some wetlands over the years. There is a high need for an updated national wetlands inventory in Sweden, using advanced methods, and recent data.

The current trends in Earth Observation (EO), and Remote Sensing (RS) are employing high-resolution satellite imagery, and replacing traditional image analysis techniques with Machine Learning (ML) algorithms (Hird et al., 2017). ML is the state-of-the-art solution for classification, and regression problems, that achieves outstanding accuracies, and bypasses traditional modeling approaches. These algorithms "learn" from data, finding patterns that might not be easily distinguishable to the human eye. Many authors argue that non-parametric Random

Forest (RF) supervised ML algorithm excel for classifying wetlands (Adam et al., 2010; Amani, Mahdavi, et al., 2019; Berhane et al., 2018; Corcoran, 2013; Hird et al., 2017; Lamb et al., 2019; Mahdianpari et al., 2019, 2020; Tian et al., 2016). Therefore, RF was adopted in this study to classify the satellite data on a pixel-wise basis. The biggest challenge for ML applied to RS is the acquisition, handling, and processing of large amounts of geospatial information (Amani, Brisco, et al., 2019; Hird et al., 2017).

Google Earth Engine (GEE) is a novel platform, hosting a multi-petabyte repository of satellite imagery. GEE facilitates the access, processing, and analysis of multi-source, and multi-temporal Analysis Ready Data (ARD) stored in the cloud (Gorelick et al., 2017). GEE allows users to incorporate locally stored data, and implement ML algorithms. GEE has been enthusiastically adopted by the scientific community for many applications, among which is wetlands monitoring (Amani, Mahdavi, et al., 2019; Chen et al., 2017, 2017; Hird et al., 2017; Lamb et al., 2019; Mahdianpari et al., 2020; Wu et al., 2019).

Therefore, the main objectives of this study are to:

I. Map wetlands all over Sweden, by employing Google Earth Engine, multi-temporal high spatial resolution satellite data from multiple sources, and Random Forests (RF) machine learning (ML) algorithm. This study will produce a new national wetlands inventory map (termed RFWI hereafter) that addresses the aforementioned VMI's limitations.

II. Evaluate the generated wetlands classification map, against the ground reference samples, in the terms of overall, user's and producer's accuracies, and Kappa coefficient.

III. Compare the developed RFWI with existing global and continental products, and discuss their similarities and differences.

2 Background

2.1 Wetlands

Wetland is defined as land that remains submerged underwater most time of the year, water is continuously, seasonally, or intermittently standing above the vegetation, or saturating the soil (Davidson, 2014; Finlayson, 1995; Gunnarsson & Löfroth, 2009; Lehner & Döll, 2004). Wetlands is a very broad term, it refers to complex ecosystems that look, and behave very differently. Wetlands are governed by their hydrology and can be subdivided into man-made, inland, and marine and coastal wetlands (Ramsar Convention Secretariat, 2016; Reddy & DeLaune, 2008). Man-made wetlands are ponds for fish, and shrimp harvesting, rice paddies, dams, reservoirs, and waste-water treatment, among other uses. Inland wetlands can be sub-divided into peatlands, bogs, fens, freshwater marshes, freshwater swamps, and riparian wetlands. While marine and coastal wetlands mainly encompass mangroves, and tidal marshes (Reddy & DeLaune, 2008).

Wetlands are everywhere, from tundras to tropical environments. Most wetlands are usually found in low topographies (Lehner & Döll, 2004), and the interface between water and upland (Reddy & DeLaune, 2008). The global area of wetlands has been estimated between 5.3 and 12.8 million km^2 (6-10% of global land area). However, it is largely agreed that acceptable figures are difficult to estimate on a global scale (Davidson, 2014; Lehner & Döll, 2004; Mitsch et al., 2013; Ramsar Convention Secretariat, 2016; Reddy & DeLaune, 2008).

According to Zedler & Kercher (2005) wetlands provide ecosystem services valued at 13,165 billion US $ per year globally, while (Batzer & Sharitz, 2007; Costanza et al., 1997) estimate that only estuaries, swamps, floodplains, tidal marshes, and coastal seagrass/algae beds (mostly marine & coastal wetlands) provide 71,316 US dollar ha^{-1} yr^{-1}, none of these amounts are fixed due to inflation. The high value of wetlands is a product of their diversity, concentrating a multitude of species (e.g. Waterfowls, rare plants, and fish) that make these ecosystems highly productive (Zedler & Kercher, 2005). Coastal wetlands minimize hazards in populated areas, critical, as we know that close to 70% of the world's population lives near coastal estuaries, and inland freshwater (Dang et al., 2020). They can alleviate the damages caused by floodings, reducing the height of the floods, and the risk of floods downstream, by storing, and slowing water (Zedler & Kercher, 2005). Wetlands can be thought of as "*living filters*" capable of transforming pollutants (Reddy & DeLaune, 2008). If water rich in nitrate-nitrogen runs off agricultural fields, it can lead to the eutrophication of water bodies, ultimately decimating fish populations, and wetlands are capable of dealing with the harmful effects of large concentrations of fertilizers (Zedler & Kercher, 2005). Modern anthropogenic activities (e.g. fossil fuels, industrialization, and deforestation, among others) have changed the constitution of the atmosphere when compared to pre-industrial estimates. By creating a surplus of gases with a greenhouse effect, e.g. Carbon Dioxide (CO_2), Methane (CH_4), and Nitrous Oxide (N_2O). It is proven that wetlands can sequestrate (remove) carbon from the atmosphere, and store it by degradation (Mitsch et al., 2013; Reddy & DeLaune, 2008; Zedler & Kercher, 2005).

Wetlands store 12% of the global carbon pool (Erwin, 2009) in a different way than forests, not

in the vegetation but mainly in the soil (Zedler & Kercher, 2005). Peatlands have been estimated to make up half of the global inland wetland area (~3% of the world's land surface), and they contain 30% of the global soil carbon (Erwin, 2009). Mitsch et al. (2013) performed a review of 14 studies and modeled carbon fluxes in several wetlands, located in temperate, and tropical climates; concluding that wetlands play a net carbon sink role, of 830 TgC/yr or 118 gC m^{-2} yr^{-1} on average.

Temperatures govern wetlands' CH_4 fluxes (Keane et al., 2021), thus, climate change, and the warming of wetlands, could accelerate climate change due to positive feedback (Davidson & Janssens, 2006). Additionally, the anaerobic conditions in waterlogged peat are favorable for methanogenesis, constituting a source of atmospheric CH_4, with a warming potential over 30 times that of CO_2 (Keane et al., 2021). However, CH_4 emissions from wetlands have been deemed "*unimportant*" by Mitsch et al. (2013) when compared to their carbon sequestration potential. Affirming that tropical wetlands (with the highest temperatures) remain a net carbon sink after balancing emissions with sequestration.

According to Davidson (2014), wetlands have been used by humans from centuries to millennia. Wetlands get drained, and degraded, because they store peat, valuable for agriculture, and other industries. The drainage of wetlands release CO_2 into the atmosphere (Zedler & Kercher, 2005). The creation of man-made wetlands has been found to be a beneficial, and recommended practice, as man-made wetlands can serve as sinks of run-off nitrogen, and atmospheric carbon (Mitsch et al., 2013; Söderqvist, 2002).

Being one of the most productive ecosystems on Earth (Ramsar Convention Secretariat, 2016) did not diminish their plummet. It is estimated that around 50% of wetlands areas have been lost due to humans (Zedler & Kercher, 2005), and activities related to agriculture are the most detrimental. The proportion of change in wetlands' extent, and quality is difficult to assess since few countries have had accurate maps for long enough periods. Davidson (2014) reviewed a total of 189 reports and concluded that today's global natural wetlands coverage is less than 80% of what it was at the start of the 18th century, with the steepest decline occurring solely during the 20th century (64-71% decrease). Moreover, natural inland wetlands were found to be at a higher risk, with global wetlands area decreasing during the 20th century estimated between 69-75% for inland, and 62-63% for marine & coastal. Such losses in wetland coverage were slowing down in Europe, and North America after 1980 (Davidson, 2014).

The services of wetlands are critical and undeniable, the identification of their location and extent constitutes a valuable asset for human life, environmental science, the mitigation of greenhouse gases, and many other applications. However, wetlands are dynamic ecosystems with changes in extent, and conditions, during a year and/or over years, which makes them difficult to map. Remote sensing is one of the best options to monitor wetlands and the only practical way to produce wetland maps at global or national scales (Adam et al., 2010; Amani, Brisco, et al., 2019; Lehner & Döll, 2004).

2.2 Satellite Remote Sensing

Remote sensing (RS) is the term for Earth Observation (EO) from afar, resembling a bird's

perspective (Chuvieco, 2016). It started when maps were made from balloons, and quickly advanced to the capture of aerial photographs, nowadays low-altitude unmanned aerial vehicles (UAVs), and satellites are employed.

RS relies on physical concepts that explain how objects react to electromagnetic (EM) radiation. Research on EM radiation, carried out by the renowned scientists Maxwell, Huygens, Planck, and Einstein (Chuvieco, 2016), lead to the discovery that photons with the same radiant energy will have an equal frequency, and wavelength. Therefore, EM radiation can be denoted by its wavelength λ (in meters) or frequency (in hertz).

It is widely accepted that the human eye works by capturing EM radiation in the visible (VIS) spectrum (λ ~ 400 to 700 nm). Nevertheless, the EM spectrum is not limited to the VIS range but spans everything known between Gamma Rays, and television wavelengths (very high frequencies), that humans cannot detect. A limited range of wavelengths is called a band. Some of the most studied bands in RS are the visible (VIS), Near-Infrared (NIR), Short-wave Infrared (SWIR), Thermal-Infrared (TIR), and microwaves (MW). The VIS spectrum (400-700 nm) can be further separated into blue (400-500 nm), green (500-600 nm), and red (600-700 nm) bands. NIR, SWIR, and TIR bands comprehend wavelengths between 700-1200 nm, 1200-8000 nm, and 8000-14000 nm, respectively. MW refers to wavelengths greater than 1 cm, used by radars, and for other purposes like heating food (Chuvieco, 2016).

Light can be thought of as EM waves (or photons) spanning many bands with high intensity in the VIS spectrum. As light hits an object, it may be reflected with equally high intensities in the three VIS bands (blue, green, and red), making it look white to humans, like snow. Colors are produced by different intensities between these three VIS bands (RGB) and originated from the interaction between light and objects, e.g. vegetation in the VIS spectrum reflects light with the highest intensity in the green band, making it look green (Chuvieco, 2016). Hence, materials that make objects have varying absorption, reflection, and transmission coefficients, that explain how they deal with specific wavelengths. These coefficients depend on a material's chemistry, and physical constitution, and apply not only for the VIS but for all the EM spectra, e.g. lead walls are used to protect x-ray operators since lead blocks the transmission of those low-frequency wavelengths, harmful to human health in the long run. One of the great advances for RS has been identifying the signature reflectance of specific objects.

Airplanes, UAVs, and satellites carry sensors that mimic and expand the functioning of the human eye, capturing information from the Earth's surface in different bands, beyond the VIS. Sensors are broadly separated into two types, passive, and active. Passive sensors capture EM radiation emitted by an external source, like the sun, and are also referred to as optical sensors (e.g. photographic cameras, and push-broom sensors used in satellites). Optical sensors have the advantage of capturing in the VIS spectrum, for true color results (resembling human vision), and in the NIR, SWIR, and TIR bands, obtaining information not perceivable by the human eye. On the other hand, active sensors capture reflections from radiation emitted by themselves (e.g. radar, lidar). Some of the advantages of radar sensors are capturing scenes during the night, the ability to penetrate clouds (that hinder the utilizable part of optical imagery), and deeper penetration into vegetation, and soil, than optical sensors (Chuvieco, 2016). And both types have

disadvantages, e.g. optical data is affected by clouds, and radar data is noisier than optical data. Sensors used for EO are engineered to capture bands from the EM spectra, with well-defined objectives, like monitoring water, vegetation, gases, and exposed rocks, among others.

Radar sensors can restrict the transmission and reception of MW signals (or waves) to the desired direction (Chuvieco, 2016), called polarization. Identic transmission-reception polarizations are called like-polarization, e.g. vertical-vertical (VV), and horizontal-horizontal (HH). Transmission and reception polarizations with a 90 degrees angle are referred to as cross-polarization, e.g. vertical-horizontal (VH), and horizontal-vertical (HV).

Some examples of satellites carrying optical sensors are MetOp, POES, TERRA, SPOT, Landsat TM, Landsat 7, and Sentinel-2, among many others. Some satellites carrying radar sensors are ERS, Radarsat, Envisat, and Sentinel-1, among others. These satellite missions have been widely adopted by researchers for monitoring wetlands, leveraging the information that underlies the reflection from objects on the ground. Table 1 summarizes the data from satellite-borne sensors exploited by relevant research regarding wetlands.

***Table 1**. Summary of satellite data employed by selected research for mapping wetlands.*

Data	Source	Reference
VIS+NIR+SWIR	Sentinel-2	Dang et al. (2020); Hird et al. (2017); Mahdianpari et al. (2020); Zhao (2020)
VIS+NIR+SWIR	Landsat (TM/8/ETM+)	Amani, Mahdavi, et al. (2019); Chen et al. (2017); Corcoran (2013)
VIS+NIR	WorldView-2	Berhane et al. (2018)
VIS+NIR	Pléiades-1B	Tian et al. (2016)
Radar (VV+VH)	Sentinel-1	Chen et al. (2017); Hird et al. (2017); Mahdianpari et al. (2019); Zhao (2020)
Radar (HH+HV)	ALOS PALSAR	Corcoran (2013)

2.3 Wetlands mapping

Wetlands have been a subject of governmental concern due to their rapid areal loss. In 1971 the Ramsar Convention of Wetlands treaty was signed by 18 nations, aware of the importance of wetlands, and committed to their conservation. Ramsar is known as the first modern multilateral environmental agreement, as of 2016, 169 member states had signed the treaty, and held conferences every three years to discuss national reports and policies regarding wetlands conservation. Ramsar is actively monitoring and inventorying wetlands, and it maintains a List of Wetlands of International Importance, made from more than 2,200 wetlands or “Ramsar Sites” that cover more than 2.14 million km^2 worldwide (Ramsar Convention Secretariat, 2016). Ramsar sites are submitted by the member states, and the methodologies vary between states.

There are many different methods, and data sources for mapping wetlands or producing wetlands inventories. In general, the data sources used for wetland mapping can be classified into three main categories: (1) field surveys, (2) aerial photographs, and (3) satellite imagery data. The following subsections briefly describe each category and provide relevant examples.

2.3.1 Field surveys and historical data

Wetlands have been visited and monitored directly on-site (Ballin et al., 2018), capturing high-fidelity data, or by gathering and merging historical/ancillary data (Lehner & Döll, 2004; Ståhl & Weimann, 2022).

The Global Lakes and Wetlands Database (GLWD) was produced by Lehner & Döll (2004), it has a 30-second resolution (or a scale between 1:1,000,000 and 1:3,000,000), and comes in three versions, the third (GLWD-3) includes wetlands. It was produced by gathering mainly GIS data, but also non-geo-referenced databases, the following datasets were employed for identifying wetlands: The Ramsar Database (2002), The digital chart of the world (1993) developed by ESRI, ArcWorld 1:3M dataset (1992) also by ESRI, Wetlands map of the World Conservation Monitoring Center WCMC (1993) from the United Nations Environment Protection (UNEP), and finally the USGS Global Land Cover Characteristics database GLCC (1991 and 2000). Lehner & Döll (2004) validated their results by comparing the number of water bodies with older global databases, and their results agree to a large extent. Nevertheless, their wetlands product (GLWD-3) does not capture wetlands' fine boundaries, and wetland areas are greatly overestimated in most regions. Moreover, the authors highlight that this dataset cannot replace ground-truth, and remote sensing in the future would enable researchers to produce better quality inventories.

The Land Use and Coverage Area frame Survey (LUCAS) is a harmonized survey of land cover (LC), and land use (among other information), captured across all of the European Union. It is produced and delivered every three years since 2006 by cooperation between the Joint Research Centre (JRC), the Agriculture Directorate General, and the European Statistical Office (EUROSTAT). Each surveyed point is in a tile of a 2 km^2 grid covering Europe, and the surveillance might be done by direct measurements in the field or in the office by photograph interpretation (Ballin et al., 2018). The objective of LUCAS is to monitor the social and economic use of land, as well as ecosystems. LUCAS possess a specific class for wetlands, and they describe them as regions inundated with water temporarily or permanently, where inhabitant plants and animals have evolved to being damp for lengthy periods.

A study carried out by Ståhl & Weimann (2022) employed historical hand-drawn maps to predict wetlands occurrence using ML algorithms. They trained with a small section in Jönköping County and predicted wetlands occurrence in all 'Southern' Sweden (it is not explicitly expressed, but from the interpretation of a figure in that study, they only excluded Jämtland, Västernorrland, Västerbotten, and Norrbotten). They found a correlation between the areas with wetlands loss, and well-developed agriculture, probably due to drainage. In their classification, the areas known to present the densest wetlands were predicted to be relatively untouched.

2.3.2 Aerial photographs

Field surveys are usually performed to confirm the interpretations made from RS imagery, e.g. VMI employed aerial photographs, but visited a tenth of the sites to obtain additional information, and corroborate the interpretations made from photographs. But large-scale field surveys with high spatial resolution, and consistent methodologies, are difficult to carry, and their re-visiting frequency is rather limited. Wetlands have been subject of RS methods since the

aerial photographs were introduced (Adam et al., 2010; Gunnarsson & Löfroth, 2009; Ozesmi & Bauer, 2002). VMI is described in more detail in Section 2.4.

One of the first recorded studies mapping wetlands from airplanes focused on freshwater marshes (Shima et al., 1976). Combining true color (RGB), and IR photographs, with data from field samples, obtained during the spring, and fall seasons. They tried to distinguish between 12 vegetation species known to exist in the region of interest. Shima et al. (1976) concluded that the differentiation from IR photographs in spring was successful only for 3 species, thanks to each plant's characteristic color tones, and specially to the ancillary knowledge of their small distance to watercourses. During fall they obtained a bigger success rate, correctly identifying 5 out of the 12 species, mostly based on the imagery. They point out that the signature reflectances of the vegetation are very similar, plus the variability in the reflection of sunlight hitting the ground, made differentiating species a difficult task, not possible employing solely aerial photographs.

Another study (Howland, 1980) aimed to differentiate wetland types within a very diverse region (where marshes, peatlands, and swamps, among others, could be found), employing true-color, IR, black & white, and multi-band photographs, with scales between 1:52,000 and 1:104,000. They found true-color photographs to be useful, while IR photographs were found to be very noisy since vegetation show patterns in the IR band different from those in the VIS. Nevertheless, the visual interpretation of textures, and canopy height, were found to be the best discriminating factors. They concluded that wetland types were easier to map than individual species. An interesting finding was that the existence of wetlands can be seen in their surroundings, an example provided was that sphagnum peatlands were concentric to other types of vegetation, and that concentricity of wetlands helped their identification (Howland, 1980).

2.3.3 Satellite imagery data

Mapping wetlands from aerial photographs is difficult, and hardly scalable, it works for small extents but is not feasible for large scales, and the revisiting frequency is limited. Land covers and land uses are dynamic, and ancillary data becomes outdated fast. Hence, RS data have been recently used for mapping global land cover (Friedl et al., 2000). Aerial photographs and satellite imagery are not very different, and research migrated from air-borne to satellite when the considerable gap in spatial resolution (that existed at the start of the millennium between both methods) shrank. Additionally, the visual methods used for identifying features in aerial photographs are not ideal for large scale studies, since computational power increased dramatically, mathematical algorithms (e.g. the maximum likelihood estimation or MLE) have been used for image segmentation, and assigning classes based on statistical information. And newer ML algorithms now outperform MLE.

The data from Landsat TM, and SPOT, was found to be unsatisfactory for classifying wetlands, and distinguishing between vegetation species (Basham May et al., 1997; McCarthy et al., 2005). These authors pointed out the need for higher spatial and spectral resolution imagery to obtain better results. After reviewing the advantages and disadvantages of satellite monitoring of wetlands with optical and radar satellites deployed between 1972-1995 (Landsat MSS, Landsat 4, Landsat 5 TM, SPOT-1,2,3,4, AVHRR, RADARSAT, ERS-1), Ozesmi & Bauer (2002) concluded that satellite imagery is specially useful for early, and continuous surveillance over

large continental or national geographies, deeming that aerial photographs and field surveys are better methods for local extents. Combining multi-source imagery was not fully exploited then. These authors reinforced the benefits, and accuracy improvements of using multi-temporal imagery. They also pointed out the promising results of rule-based algorithms excel statistical classifications (like MLE). And that separating wetlands from other land cover (LC) classes based on ancillary data should be performed if possible.

The release of data from the Moderate Resolution Imaging Spectroradiometer (MODIS) whisk-broom sensor, on-board of the Terra satellite, increased the spatial and temporal resolution, and quality of LC products (Friedl et al., 2000; Huete et al., 2002). That previously relied on data from the AVHRR (Advanced Very High-Resolution Radiometer) and used MLE for classifying it. MODIS is currently produced with a spatial resolution that oscillates 500 m (Friedl et al., 2010). MODIS LC products differentiate wetlands from other land covers.

Hird et al. (2017) studied a 13,700 km^2 extent in Alberta (Canada), highly dominated by wetlands. Aiming to classify multi-source imagery from Google Earth Engine, as one of three classes: water bodies, dry land, or wetlands; employing a Boosted Regression Tree (BRT) ML algorithm for the task, on a pixel-basis. A very similar approach to our study. The multi-source imagery used was composed of Sentinel-2 optical imagery, Sentinel-1 radar imagery, high-resolution elevation models, and field samples from a third party. They created a binary wet-dry product that had an 85% OA to Alberta's wetlands inventory. Hird et al. (2017) found radar, and topographical data to be among the most important data for the classification of wetlands using ML. They indicate that the algorithms used for computing topographical indices created uncertainty in their results.

Amani, Mahdavi, et al. (2019) generated the *"first"* Canada-wide wetlands map, by classifying multi-temporal composites from 29,456 Landsat-8 images (VIS, NIR & SWIR bands), with Random Forest (RF), in a pixel-wise manner. Canada encompasses 9.985 million km^2, the gathered field samples covered 798.6 km^2 in total, 448.7 km^2 belonging to wetlands, from 5 of the 13 Canadian states, separated 50/50 for training and evaluating the classification accuracy. Achieving an overall accuracy of 71%, and a kappa coefficient of 0.670, while the producer's, and user's accuracy were 66%, and 63%, respectively. Their non-wetland classes got an overall higher accuracy than wetlands, but this was an expected result, since the complex nature of wetlands, and their high variability both in time and space makes mapping them a challenge. The spectral signature of different wetland classes overlap in different wavelengths. Moreover, any of the five wetland classes they used could be further subdivided, explaining multi-modal trends in single classes. Among other issues acknowledged by authors, a fairly small amount of field samples compared to Canada's size was used, increasing the number of field samples produces better quality and more dependable results. Additionally, only Landsat-8 imagery was employed as input for the classifier, the overall accuracies are expected to raise when combining optical imagery with Synthetic Aperture Radar (SAR), topographic, textural, and ancillary data (Adam et al., 2010; Amani, Mahdavi, et al., 2019; Mahdianpari et al., 2020; Ozesmi & Bauer, 2002).

Mahdianpari et al. (2020) also generated a Canada-wide wetlands map, reporting an overall

accuracy approaching 80%, combining multi-year multi-source imagery from Sentinel-1 (13,519 images), and Sentinel-2 (51,060 images) hosted in GEE. Classifying with a RF ML algorithm based on an object-based segmentation (instead of pixel-wise basis), in GEE. They gathered 8,904 (3,727 from wetlands) in-situ field samples (polygons bigger than 1 ha) from earlier surveys.

Most authors coincide in cloud and snow, covering large extents during winter, and spring, to be one of the main challenges of using optical imagery, affecting the utilizable portion of images.

The ESA WorldCover Consortium delivered (2020) a global LC dataset with 10 m spatial resolution, called the ESA WorldCover product. WorldCover is one of the latest global LC datasets with high spatial resolution and is freely available. It was developed by classifying satellite imagery from the Sentinel-1 & Sentinel-2 satellite missions, using a (ML) gradient boosting decision tree (CatBoost) algorithm (ESA, 2020). WorldCover is reported to have a 75% accuracy, validated against 21,000 primary sampling units, made of a hundred 10x10 m pixels each, where at least 3,000 had to be in each continent (ESA, 2021). It was also visually compared to two robust LC products with the same spatial resolution: FROM-GLC10, and ESRI 2020 Land Cover. Among the 11 classes of WorldCover, herbaceous wetlands, and mangroves can be grouped into wetlands.

2.4 Sweden's National Wetland Inventory (VMI)

Sweden's country-wide wetlands inventory called VMI by its acronym in Swedish (*Våtmarksinventeringen)* was the product of a cooperative effort between the Swedish Environmental Protection Agency (*Naturvårdsverket*), and environmental protection agencies from each county. One of VMI's strengths is that the involved agencies followed a common methodology, standardizing the data quality, and fidelity. It took 25 years to attain its objectives, starting in 1981 and finishing in 2005 (Gunnarsson et al., 2014; Gunnarsson & Löfroth, 2009). The definition of wetlands, used for the production of VMI coincides with most authors (Section 2.1), but with a few differences, i.e. open-water areas are not part of VMI, differing from Ramsar's definition. Additionally, 50% of the vegetation present in the wetlands needs to be hydrophilic, excluding the case of temporarily exposed lake-, sea-, and river- beds, which are included in VMI regardless of the lack of vegetation. During this time, approximately 35 thousand wetlands were surveyed, located in continental land, and coastal areas belonging to Sweden, covering approximately 43,000 km^2 (~10% of Sweden's land area).

The acquisition of aerial photographs and the identification of wetlands from the photographs was the first step in VMI's methodology. The selection of wetlands included in VMI was based on their size since many counties did not have the financial resources to map the smaller wetlands. VMI only includes wetlands bigger than 10 hectares (ha) in the countries south of, and including Västra Götaland, Örebro, Västmanland, and Gävleborg (Appendix A Figure A.1), where the photographs used had a 1:30,000 scale. Note that the counties and their boundaries at the moment of VMI's realization were different from the current. Parts of Örebro, Värmanlands, and Dalarna mapped only wetlands bigger than 20-25 ha. While Jämtland, Västernorrland, Västerbotten, and Norrbotten only mapped wetlands bigger than 50 ha since the photographs had a 1:60,000 scale (Appendix A Figure A.1). Only wetlands in low elevations were

considered, excluding wetlands from the alpine regions.

Afterward, wetlands were classified for step 2, based on their "*nature conservation*", following 5 criteria: representativeness, size, untouched-ness, diversity, and rarity. And split into 4 classes: (1) very high-, (2) high-, (3) some- (high to low), and (4) low- nature conservation, The distribution in such classes is 11%-, 24%-, 51%-, and 14%- of the surveyed wetlands, respectively. Destroyed wetlands are not included in the inventory but destroyed sub-sites of larger wetlands are mapped (Gunnarsson et al., 2014).

Step 3 was the final, it mixed field surveillance, and describing the wetlands. Approximately 12% of the wetlands were visited, specifically the most valuables (belonging to classes 1 & 2). And the wetlands were briefly described based on internationally accepted subtypes. VMI survey found that the most common wetland types in Sweden are bogs in the south; while fens, and mixed mires dominate the north. Topogenous fens, string mixed mires, and string fens are the most common wetlands type in Sweden, and their distribution is mostly dependent on climate change through time, and human activities (Gunnarsson et al., 2014). Only about 8,600 km^2 (~20%) of the wetland's area is completely unaltered, and humans occupy the first place in wetlands destruction.

VMI is finished and newer revisions with the original methodology are not planned by the Swedish Environmental Protection Agency. Nonetheless, a new inventory based on more recent data is a work in progress, this information was obtained via direct communication with the agency.

2.5 Google-Earth-Engine (GEE)

Google Earth Engine (GEE) is a cloud environment with a data catalog of satellite imagery at a petabyte-scale, developed, and hosted by Google Inc. It enables RS scientists, and also a much wider audience, to a planetary-scale tool that not only hosts data, but allows its processing, and analysis, within the same environment, thanks to a high-performance computation service (Gorelick et al., 2017). More than 6,000 scenes (or images) from active satellite missions are included in GEE daily, with a lag close to 24 hours from their capture (Gorelick et al., 2017). Researchers struggled in former times with the lack of freely available satellite imagery (Adam et al., 2010). The data hosted in GEE is gathered by Google Inc. and acquired directly from the producers, e.g. NASA, and ESA, among others. Additionally, GEE gives users the ability to also upload, and merge their own data with the public data catalog, for more advanced problems. Also, the user can combine imagery with vectorial data, in different types of operations. Some examples of RS imagery hosted in GEE are: Landsat 4/5/7/8 surface reflectance, Sentinel-1 GRD, Sentinel-2 MSI, MODIS (surface reflectance, LC, vegetation indices, among others); Table 1 in Gorelick et al. (2017) provides a wider list, with additional information.

In GEE argot, images/scenes captured by a single sensor, or features of a vectorial dataset are grouped in collections, and the metadata of each feature in a collection allows users to filter, clip, and apply many other functions to subsets. GEE has a wide range of per-pixel / per-feature functions, neighborhood operators (e.g. for slope and texture), as well as aggregators that work in the time dimension (e.g. calculating the pixel-wise mean of N overlapping images).

Numerical and array operations, ML, and visualization capabilities can be found in GEE. The basis behind GEE's functioning is out of the scope of this study and is thoroughly explained by Gorelick et al. (2017).

GEE can be accessed by the user through a GUI hosted in a webpage (Google, n.d.-a) called code editor, which accepts JavaScript code for accessing satellite imagery collections, and for any of GEE's functionalities, it includes a map where the data can be visualized. Another option is accessing GEE through python, but the user requires specialized libraries and a Jupyter Notebook for visualization. For both the code editor, and python, a Google account is required to access the GEE service, and special permissions need to be granted by Google. To the current date, the service is tailored to academic users, and the basis for commercial users is not yet defined.

Due to the large ARD catalog accessible within GEE, it has been widely adopted in recent years by researchers, for a wide range of applications like global forest change, global water change, wetlands mapping, rice paddy mapping, mangroves mapping, flood mapping, crop yield estimation, urban mapping, among others (Amani, Mahdavi, et al., 2019; Chen et al., 2017; Gorelick et al., 2017; Hird et al., 2017; Mahdianpari et al., 2020; Wu et al., 2019). Most of which are using ML classification algorithms like Random Forest (RF). Training a ML classifier in GEE poses two limitations, at most 1 million observations can be used for training a classifier, and their weight cannot exceed 100 MB.

2.6 Machine Learning

Machine Learning (ML) is programming a computer to learn from data, by making it iterate through a task or process while attempting to minimize/reduce the error of the last iteration (Géron, 2019). ML applications span a very wide range of fields and are specially adopted in image analysis. There is also a wide range of ML algorithms (models), that work differently but can solve regression (regressors), and classification (classifiers) tasks.

The way that a ML algorithm learns from the data might be supervised or unsupervised. Supervised learning requires human intervention for describing (labeling) the desired results e.g. a binary answer like yes or no, the breed of a dog, a nominal value, or class; this desired result is called a label. Some types of renowned supervised ML algorithms are Decision Trees (DT), Random Forest (RF), Support Vector Machines (SVMs), and Neural Networks (NN). On the other hand, unsupervised learning relies on the machine for grouping observations into clusters (classes), e.g. K-Means clustering, Principal Component Analysis (PCA), and Isolation Forests.

ML algorithms require a lot of data to learn, usually millions of samples (Géron, 2019), and high-quality labels are crucial for successful results. Generally, the data is split 50/50, 40/60, or 60/40 into training/validation sets. The training set refers to the samples/observations used by the algorithm to learn from, and the validation set is used for assessing the performance of the trained algorithm, by predicting with data it did not use to learn. If the algorithm can correctly predict the labels of validation data, the results are deemed accurate, and one usual method for describing the accuracy is confusion/error matrices (more details in Section 3.5). Before training a ML algorithm, the distribution of the data plays an important role, some algorithms are

parametric (e.g. NN), requiring scaled, and sometimes normalized data. Some algorithms are non-parametric (e.g. RF), for which the data needs no prior preparation. Another important consideration to take is the possibility of the algorithm over-fitting the data, this means that it learns how to classify or make a regression only for the training data, fitting to noise, and not to patterns, ultimately hindering the possibility of extrapolating the models to other data (Géron, 2019).

The Random Forests (RF) algorithm has been widely used in recent research as a classifier, for mapping vegetation, and wetlands (Amani, Brisco, et al., 2019; Amani, Mahdavi, et al., 2019; Amoakoh et al., 2021; Berhane et al., 2018; Corcoran, 2013; Ghorbanian et al., 2021; Mahdianpari et al., 2020; Teluguntla et al., 2018). RF is an ensemble algorithm, made of many decision trees (DT), i.e. RF aggregates the prediction from a multitude of DT. RF was introduced by Breiman (2001), as an ensemble of an N number (number of trees) of DTs, that take (at random) a small group of input variables in each split node (variables per split), e.g. every tree use a sub-set of the training samples (bag fraction). The number of leaf nodes can be limited, to include at least the desired amount of training samples (leaf population). And the maximum number of leaf nodes can also be limited (max nodes). Thus, multiple parameters can be tweaked for the DTs making a RF (number of trees, variables per split, bag fraction, leaf population, max nodes), the process of testing different parameters is referred to as hyper-parameter tuning.

The term decision trees (DT) is used for algorithms with a tree-like architecture (Figure 1), where the nodes can be splits or leaves. Split nodes are conditions or rules, (like an if-statement), and which child node will be evaluated after a split node depends on the answer to the condition. Leaf nodes do not have a child and dictate the class to be assigned. Figure 1 illustrates how a DT works, if a value N is being evaluated, the first node is at depth 0, if N is lesser than 10, the next node is a leaf node at depth 1, and the N value is classified as Low. If N is greater than 10, it is evaluated again against 50, in the split node at depth 1. If N is smaller than 50, it is classified as Mild, otherwise, it is classified as High. In ML, the rules are set by the algorithm.

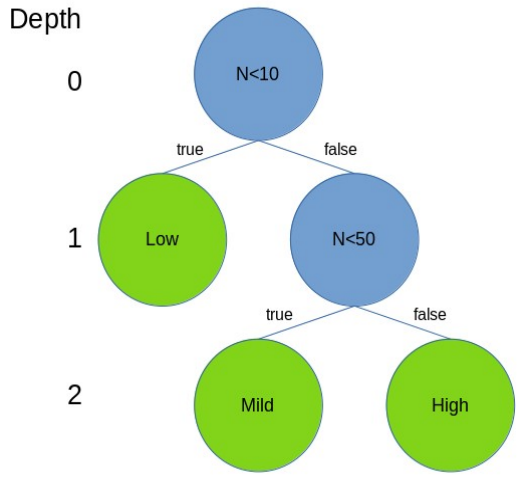

***Figure 1**. Decision Tree example. Split nodes are colored blue, and leaf nodes are colored green.*

After the DTs that make a RF are generated (by randomly assigning rules, and selecting the bags), the user receives a single result from the ensemble of DTs, this is achieved by the aggregation of the predictions from every tree. The samples that did not go into the training bag (out-of-bag), are used to estimate the error during the training. The training data is used to weigh what trees are improving accuracies the most (reducing the loss or error), and the variables in those trees can be summarized in the feature importance (Breiman, 2001; Géron, 2019; Google, n.d.-b).

The ensemble nature of RF overcomes the problem of DT over-fitting the training data because an ensemble of DT (e.g. RF) cannot over-fit (Breiman, 2001; Géron, 2019). And using more trees than required is also encouraged due to RF not being able to over fit. Other advantages of RF are the outstanding accuracies it can achieve, no need for data pre-processing, rapid training on large datasets, and the out of the bag accuracy being unbiased (Breiman, 2001; Géron, 2019).

Multiple studies have compared the performance of older parametric algorithms (e.g. MLE) versus non-parametric ML algorithms like RF, for LC classification purposes. And agree that RF performs better than MLE (Huang et al., 2002; Rana & Venkata Suryanarayana, 2020).

3 Data and methodology

3.1 Study Area

The region of interest is Sweden (Figure 2), which encompasses an area of 449,970 km^2. Sweden is the biggest country in the Scandinavian peninsula, north of Europe. Sweden shares borders with the countries of Norway, Finland, and Denmark, and the Baltic, Skagerrak, and Kattegat Seas. Its climate according to the Köppen-Geiger classification method (Beck et al., 2018) is mostly cold without a dry season, with warm summer (Dfb) south of Gävleborg, and Dalarna, and cold summer (Dfc) in the north. The Alpine region in the north is classified as Polar Tundra (ET). Sweden is divided into 21 counties, whose areas range from 3,046.02 km^2 (Blekinge) to 105,924.95 km^2 (Norrbotten).

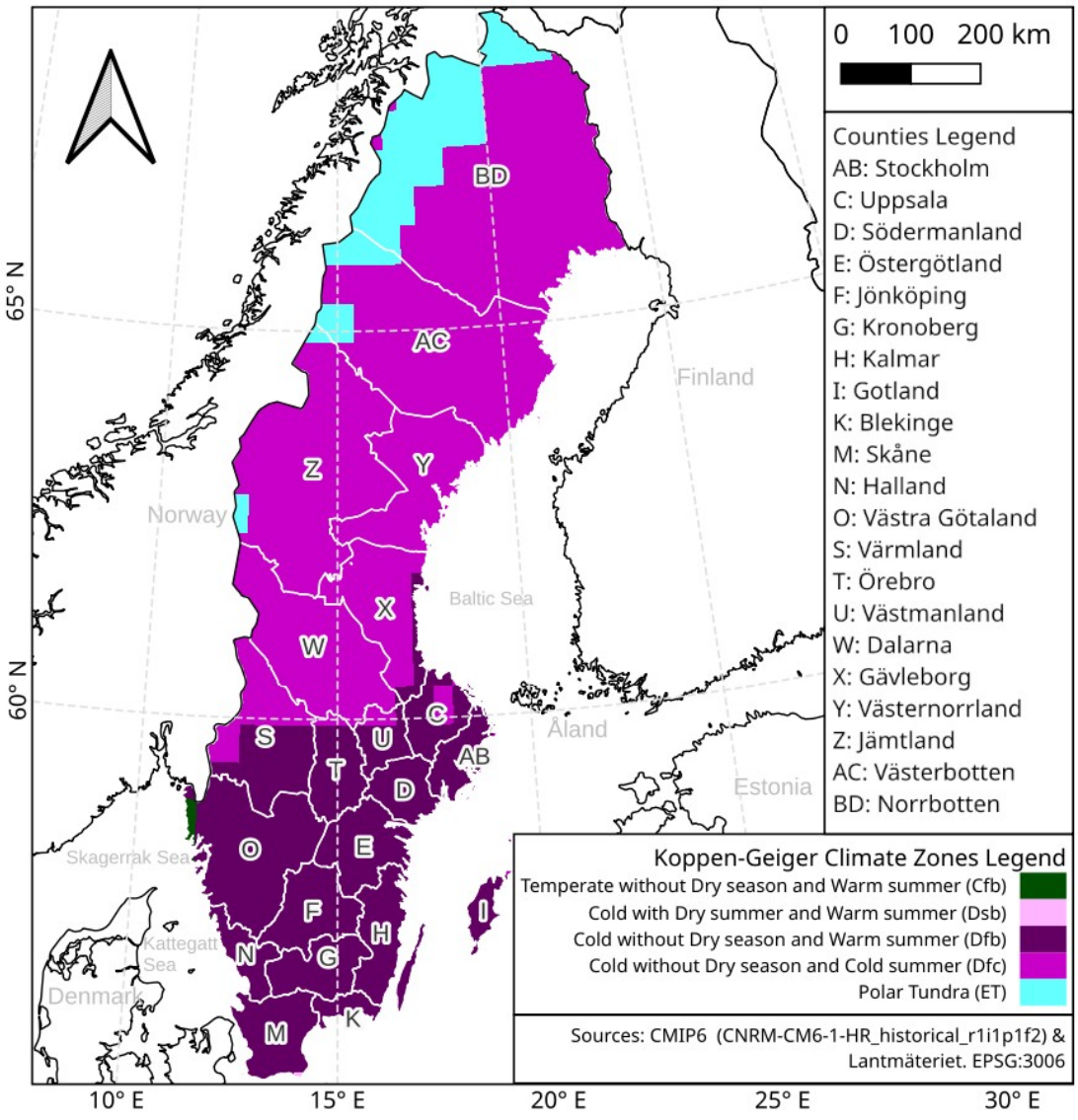

Figure 2. *Map of Sweden with Köppen-Geiger climate zones, black lines for neighboring countries, and white outlines for Swedish counties.*

3.2 Data and pre-processing

The general idea to be followed for meeting the main objectives of the study is to feed a classifier with RS satellite data from multiple sources. A classifier might be fed during the training, the validation, or for classifying unlabeled data. The word input refers to data feeding a classifier. The prediction input solely contains optical and radar satellite imagery, and topographical data. While the training input and validation sets also include labels, the first for the classifier to learn, and the second for assessing how accurate the trained classifier is. After a classifier is trained, it can be used to classify every single pixel of the input imagery, generating the new wetlands inventory RFWI. The selection of inputs was the product of research review, and trial and testing.

The workflow followed from the data gathering and preparation until the RF classification of the multi-source multi-temporal imagery is illustrated in Figure 3. Note that the stratified sampling algorithm, used only for training, is performed with two different labeling methods, further developed in section 3.3. Operations performed on data hosted in GEE are briefly described in the figure, for broader descriptions refer to sections 3.2.2, and 3.2.3.

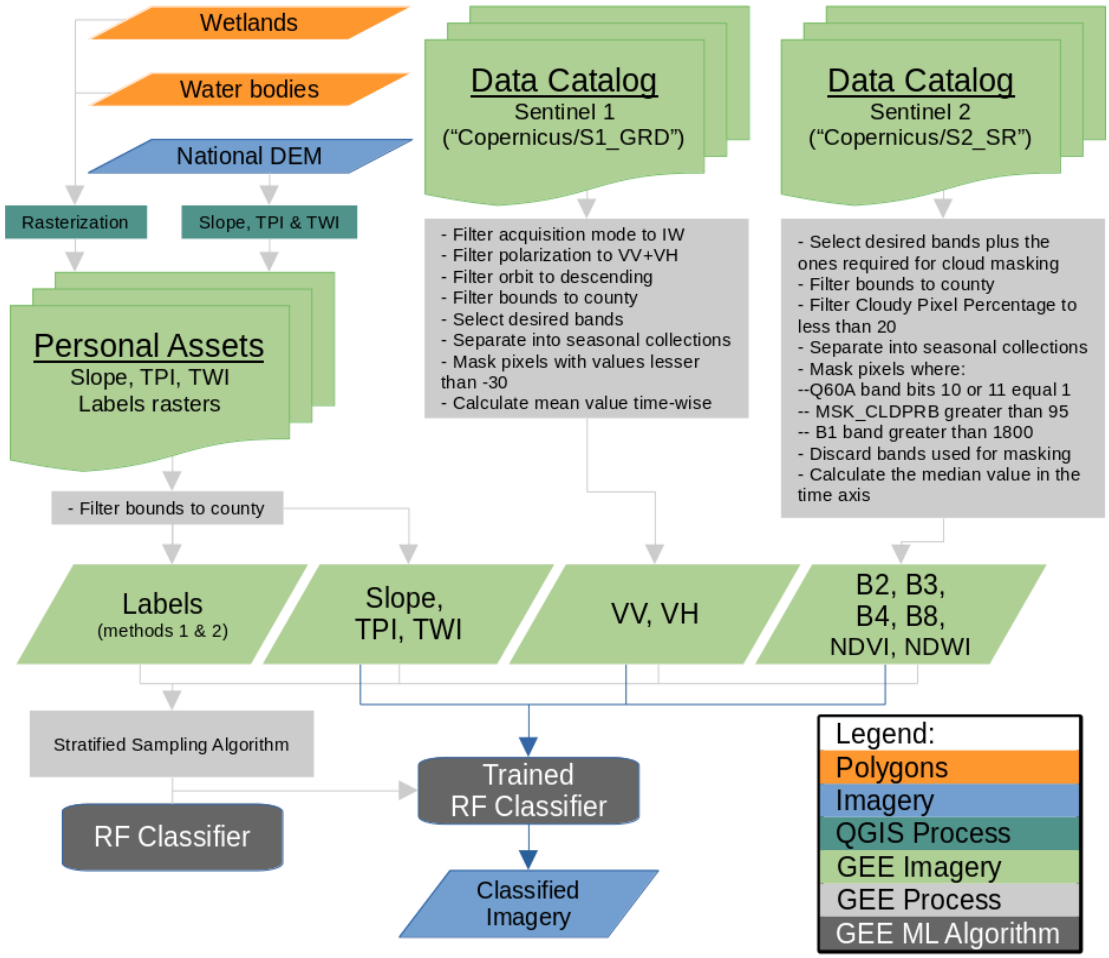

***Figure 3**. General workflow. The stratified sampling algorithm outputs points, used for training the RF Classifier. The blue arrows indicate that the trained RF Classifier is used to classify every pixel from the selected inputs. 'Copernicus/S2_SR' and 'Copernicus/S1_GRD' refer to the satellite imagery entry in GEE's data catalog.*

The scripts developed during this study, for both the GEE workflow, and the posterior analysis, are open-source (https://github.com/salvah22/wetlands-monitoring-gee).

Table 2. *Summary of datasets used during this study (VV: Vertical-Vertical, VH: Vertical-Horizontal, Blue B2: Blue, B3: Green, B4: Red, B8: NIR, TPI: Topographic Position Index, TWI: Topographic Wetness Index).*

Dataset	Description	Use
VMI	Wetlands data in form of polygons	Label input: wetlands, Digitization & comparison
Översiktskartan	Water data in form of polygons	Label input: water
Sentinel 2 MSI	Optical Imagery (~10m spatial resolution), in raster format	Data input: B2, B3, B4, B8 Derived inputs: NDVI, NDWI
Sentinel 1 SAR GRD	Radar Imagery (~10m spatial resolution), in raster format	Data input: VV, VH
Grid 50+ (GSD-Elevation 2020 Data)	Topographic data (~50m spatial resolution), in raster format	Derived inputs: Slope, TPI, TWI
Grid 2+ GSD-Elevation 2019 Data)	Topographic data (~2m spatial resolution), in raster format	Evaluation of benefits from higher spatial resolution data
ESA WorldCover	LC raster (~10m spatial resolution)	Comparison
MODIS LC1	LC raster (~500m spatial resolution)	Comparison
Ramsar Database	Wetlands data in form of polygons	Comparison
LUCAS	LC data in form of points	Comparison

3.2.1 Labeled Data

Supervised ML algorithms require labeled data to train, this means that each pixel used as training input must have a land cover class. Labels are also required for assessing the accuracy of the classifier in the evaluation step. They are commonly field data or hand-picked samples from Google Earth, also called ground-truth, with corroborated validity.

In this study, VMI was employed for identifying pixels as wetlands, it is distributed as vector polygons (Naturvårdsverket, n.d.). This dataset is composed of 34,614 polygons that make up 43,242 km^2, approximately 9.61% of Sweden's land, the distribution per county is in Chapter 4, Table 4. A distinction between wetland types (mire, fen, bog, etc.) for this study was not possible, because despite each polygon being delivered with a string attribute, containing information about the wetland, 48% of the area covered by VMI does not have a type. Additionally, most counties present only one wetland type (Appendix A Figure A.4) in VMI.

Since wetlands are usually found in transitional zones between aquatic and land ecosystems, and many VMI polygons were observed to overlap water bodies, it was considered beneficial to include water bodies as a separate class. Lantmäteriet's Vectorial Dataset General Map (Overview Map), more specifically Översiktskartan's (Lantmäteriet, n.d.-c) water polygons (*ms_riks*), were employed for labeling inland water bodies. The third class of non-wetlands was used to capture all the remaining features (urban, built-up, other vegetation, croplands, farmlands, forests, etc).

3.2.2 Optical satellite imagery data

The first set of inputs used for training, and classifying wetlands, non-wetlands, and water bodies is optical satellite imagery from Sentinel-2 (S2), specifically Level-2A Surface or Bottom of Atmosphere (BOA) Reflectances. This mission comprises two identical (A & B) satellites at an altitude of 15,000 km, phased 180° from each other to decrease the revisit time from 10 days to 5 days (European Space Agency, 2015). These satellites contain the same passive push-broom sensor, a Multispectral Instrument (MSI) that captures 10 wavelengths in the VIS-NIR, and 3 in the SWIR wavelengths of the EM spectrum. MSI imagery has 10 m spatial resolution in the bands used in this study. These MSI bands have been widely used for EO and RS applications, as well as input for ML algorithms (Dang et al., 2020; Hird et al., 2017; Lamb et al., 2019; Mahdianpari et al., 2020). From this sensor, a total of 2,949 images with less than 20 percent of cloudy pixels covering Sweden, were captured during the summer season of 2021, between June 1st (inclusive) and September 1st (non-inclusive). All those images were employed in this study (Figure 4, left). For each image, the blue (B2: 490±32.5 nm), green (B3: 560±17.5 nm), red (B4: 665±15 nm), and NIR (B8: 842±57.5 nm) bands were used. Table 3 presents the number of satellite images used for each county in Sweden, ranging from 18 images in Blekinge to 473 in Norrbotten.

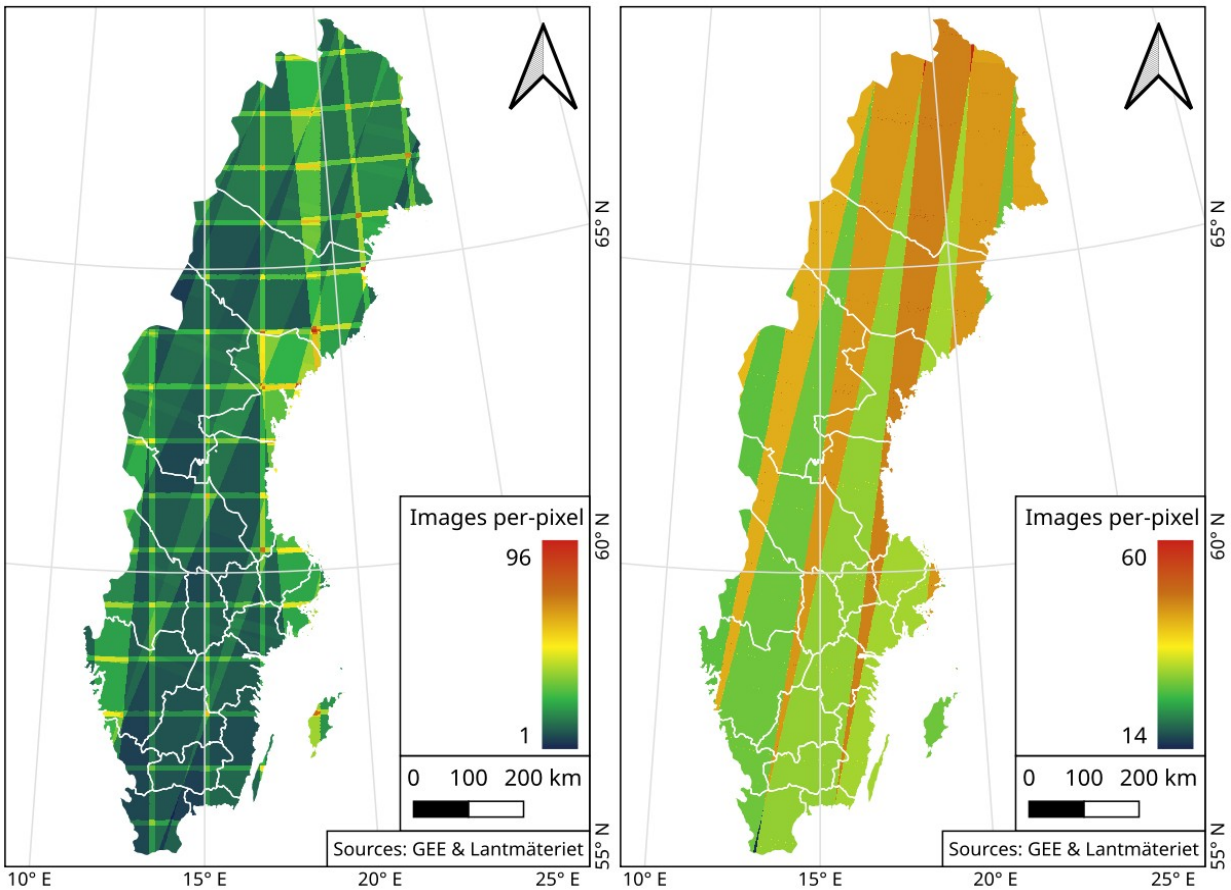

Figure 4. *Employed Sentinel-2 MSI imagery with cloud cover of less than 20% (Left), and Sentinel-1 IW descending orbit imagery (Right) available in GEE, dating from June to August (both inclusive) 2021.*

This satellite constellation follows a sun-synchronous orbit, ensuring a constant light incidence

angle from the sun on the same ground coordinates. S2 Level-2A Surface Reflectances in GEE are directly provided by Copernicus Scihub (Google, n.d.-e). The European Spatial Agency (ESA) is distributing ARD S2 BOA scenes since 2018, by applying atmospheric, terrain, and cirrus corrections to Top of the Atmosphere (TOA) Level 1C images.

Table 3. *Data per-county employed as input (NW, We & Wa: non-wetlands, wetlands, and water area digitized for LM2, respectively. S1 & S2: number of images used from Sentinel-1 & Sentinel-2 satellite missions, respectively).*

County	NW	We	Wa	S2	S1
Stockholm	35.50	3.33	28.38	86	124
Uppsala	12.63	3.07	24.88	111	111
Södermanland	11.76	4.18	9.49	47	94
Östergötland	52.62	5.37	90.31	94	108
Jönköping	7.92	12.16	24.77	90	62
Kronoberg	23.59	4.49	22.30	115	60
Kalmar	18.72	4.56	4.88	94	74
Gotland	32.14	7.32	10.48	58	93
Blekinge	16.70	2.96	3.25	47	18
Skåne	16.61	3.95	11.45	83	46
Halland	6.57	3.89	9.31	82	57
Västra Götaland	32.80	19.36	44.57	126	135
Värmland	13.32	6.80	39.92	118	114
Örebro	8.21	7.29	63.16	82	44
Västmanland	21.16	5.05	26.41	94	59
Dalarna	8.75	5.59	45.39	165	168
Gävleborg	5.97	5.01	30.31	115	217
Västernorrland	8.06	4.30	23.06	129	256
Jämtland	4.86	3.38	9.67	197	235
Västerbotten	23.59	4.81	10.54	215	336
Norrbotten	11.52	7.44	82.92	354	473

The imagery was pixel-wise masked three times, first with the provided quality band (QA60), containing information about cloud or cirrus pixels. Then the aerosols band (B1) that is sensitive to clouds (Hird et al., 2017; Mahdianpari et al., 2020), was used to mask pixels that exceed a Surface Reflectance threshold of 1800. Finally, the provided Cloud Probability Map mask was further used to filter pixels with a cloud probability greater than 5%.

Finally, the band-wise median of overlapping non-masked pixels was computed. Multi-temporal composites overcome the presence of clouds, and their shadows (Mahdianpari et al., 2020). Additionally, classifications based on multi-temporal data have been found to improve the overall accuracies (Corcoran, 2013; Mahdianpari et al., 2020; Ozesmi & Bauer, 2002). This specially applies to dynamic systems such as wetlands, whose extent, and reflectances can vary depending on the season (Zhao, 2020).

In addition to the direct measurements from the MSI sensor, the Normalized Difference Vegetation Index (NDVI) (Eq. 1) and Normalized Difference Water Index (NDWI) (Eq. 2) were computed and used as input for the classification of wetlands.

$$NDVI = \frac{NIR - Red}{NIR + Red} \quad (1)$$

$$NDWI = \frac{Green - NIR}{Green + NIR} \quad (2)$$

where NIR, Red, and Green are the surface reflectances from the near-infrared band (B8), red band (B4), and green band (B3) from Sentinel-2 satellite imagery, respectively.

Vegetation signature reflectance in the NIR increases gradually depending on the biomass, while in the Red wavelength it is very low and constant, therefore, NDVI has been employed successfully for quantifying changes in biomass (Chuvieco, 2016). A similar phenomenon occurs for water bodies when comparing reflectances in the Green and NIR bands, therefore NDWI helps in differentiating land from water (Hird et al., 2017). Both NDVI and NDWI have been used for wetland mapping in previous studies (Hird et al., 2017; Mahdianpari et al., 2019), and recommended by other authors (Amani, Brisco, et al., 2019).

Rana & Venkata Suryanarayana (2020) carried out a study where they compared the correlation, and covariance between Sentinel-2 (S2) bands, and applied a principal component analysis (PCA) to assess how many of them capture the most information. They found that S2 bands 6, 7, 8 & 8A (Vegetation Red Edge and NIR) are highly correlated, the same applies to the group of bands 2, 3, 4, 5, 11 & 12, (VIS & SWIR). Using all of the S2 bands did not contribute more information than a combination of some bands from these two groups.

3.2.3 Radar satellite imagery data

Radar imagery from the Sentinel-1 (S1) satellite, specifically from the C-band (wavelength λ~5.55 cm) Synthetic Aperture Radar (SAR) Ground Range (GRD), with 10 m spatial resolution, was included in the set of inputs. The C-band wavelength (likewise the H-Band, from other sensors) is particularly beneficial for inundated vegetation classifications, since they successfully traverse dense canopies, and carries information about soil moisture, and inundated extents (Corcoran, 2013; Podest & McCartney, 2019; Zhao, 2020).

SAR imagery is unaffected by cloudy conditions or shadows (Chen et al., 2017; Chuvieco, 2016; Corcoran, 2013; Zhao, 2020). Nevertheless, artifacts can appear in some scenes, thus values less than -30 dB were masked out, as recommended in the GEE Sentinel-1 data catalog entry (Google, n.d.-d). Then, the band-wise mean of overlapping non-masked pixels was computed.

GEE provides ARD pre-processed scenes (Google, n.d.-d), with thermal noise removal, radiometric calibration, and terrain correction. Using SRTM30 (Shuttle Radar Topography Mission ~30m spatial resolution) for latitudes less than 60, and ASTER (Advanced Spaceborne Thermal Emission and Reflection Radiometer) Global DEM (Digital Elevation Model) for the latitudes greater than 60. The employed dataset (S1_GRD) was delivered in decibels (logarithmic scale).

A total of 1,439 images containing the Vertical transmit Vertical receive (VV), and Vertical transmit Horizontal receive (VH) polarization bands, captured Sweden between June 1st, and August 31st, 2021 (Figure 4). All those images were used during this study. These polarizations

are specific to the Interferometric Wide Swath (IW) acquisition mode and follow a descending orbit path. Table 3 shows the number of S1 images used for each county in Sweden, Blekinge had the lowest (47), and Norrbotten the highest (354).

Sentinel-1 also captures Horizontal transmit Horizontal receive (HH), and Horizontal transmit Vertical receive (HV) polarizations, with the Extra Wide Swath (EW) acquisition mode. HH has been proven to successfully differentiate inundated from dry canopies (Podest & McCartney, 2019), and was found to be the most suitable SAR observation for wetland mapping (Mahdianpari et al., 2020). Unfortunately, employing those polarizations as inputs was not feasible, because this acquisition mode from Sentinel-1 satellite missions (EW) is primarily focused on monitoring maritime, ice, and polar zones (European Space Agency, n.d.-b). Hence, it only captures Sweden partly, to monitor the Baltic Sea (European Space Agency, n.d.-a) solely during the northern winter, resulting in zero images from summer.

3.2.4 Topographical data

Topographic information was found to be beneficial for wetlands classification in previous studies, added as a set of inputs (Berhane et al., 2018; Corcoran, 2013; Hird et al., 2017), or to mask data based on high elevations or steep slopes (Chen et al., 2017). Its use is also suggested by Adam et al. (2010) & Amani, Mahdavi, et al. (2019). Thus, topographical data were included in this study as a set of three inputs. More specifically, Slope, Topographic Position Index (TPI), and Topographic Wetness Index (TWI), were derived from the elevation data.

Lantmäteriet's National Digital Elevation Model (DEM) of Sweden, was used as the data source for elevation. More specifically, the Grid 50+ (GSD-Elevation 2020 data) nation-wide raster product (Lantmäteriet, n.d.-b), with a spatial resolution of ~50 m, and a 32,000 x 16,000 shape was employed for this study. It was surveyed between 2010, and 2020, the elevations range between -36.66, and 1,988.62 meters, with a mean of 303.25 m. Missing data can be found in continental Sweden, where big lakes are located (Appendix A Figure A.2). Grid 50+ is derived from a 1 m spatial resolution grid (original National Elevation Model), corresponding to the original shape of the data acquisition. The original data is acquired via Aerial Laser Scanning (LLS), which has an accuracy of 0.1 m in height, and 0.3 m in the plane, and via Aerial Image Matching (FBM) with an accuracy of 0.4 m in height (Lantmäteriet, 2019). Due to fact that the employed product is derived via step-wise bilinear interpolations, from 1m to 5m, from 5m to 10m, to 20m, to finally 50m (Lantmäteriet, 2021), the errors are stated to be 1.0 times the spatial resolution in the plane, and 1.5 times the spatial resolution in height. Hence, the dataset resolution is 50±50 m in the plane, and 50±75 m in height.

The slope was added to the set of inputs, this is not a common practice based on the research review, excluding some exceptions (Chen et al., 2017; Corcoran, 2013; Dang et al., 2020). The slope was calculated following Horn's method (Horn, 1981) using GDAL (Geospatial Data Abstraction Library), where the slope of a cell is calculated in kernels (Figure 5) and depends only on the values of the 8 nearest cells (Eq. 3). Note that the 4 closest cells (B, D, E, G) are weighted twice as the diagonals (A, C, F, H). Slope values of Sweden ranged from 0 to 65.62 degrees, with a mean of 3.38 and a standard deviation (SD) of 4.16.

A	B	C
D	Cell	E
F	G	H

***Figure 5**. Kernel for calculating a Cell's slope.*

$$dz/dx = \frac{(C+2E+H)-(A+2D+F)}{8}$$

$$dz/dy = \frac{(A+2B+C)-(F+2G+H)}{8}$$

$$slope = \sqrt{(dz/dx)^2+(dz/dy)^2} \quad (3)$$

where every letter from A to H represents the elevation of one neighboring cell of the central cell, dz/dx is the slope in the X-axis and dz/dy is the slope in the Y-axis.

TPI is the difference between a height and the mean of neighboring cells (Eq. 4), negative values can be thought of as valleys, and positive ones as peaks. It was also computed using GDAL, for each cell from its 8 closest cells (OSGEO, n.d.), i.e. 3x3 (150x150m) kernels, as small kernels are suggested (Hird et al., 2017), therefore TPI can capture local topographical variations, and allow TWI to incorporate regional-scale information. TPI values ranged between -28.76 and 50.64, with a mean of 0 and a SD of 1.16.

$$TPI = Z - \bar{Z} \quad (4)$$

where Z is a cell's height, and $\bar{Z}$ the mean of the neighboring cells.

TWI was computed using GRASS GIS function *r.watershed* (distributed along with QGIS), as in Eq. 5. TWI values ranged 2.00 and 32.97, where the mean is 9.64 and the SD is 4.16.

$$TWI = \ln\left(\frac{\alpha}{\tan(\beta)}\right) \quad (5)$$

where α is the cumulative up-slope area draining through the cell per unit contour length, and tan(β) is the local slope angle (OSGEO, 2022).

The Grid 2+ (GSD-Elevation 2019 data) dataset, with a spatial resolution of ~2 m was acquired (Lantmäteriet, n.d.-a) for assessing the benefits of very high spatial resolution data. Due to computational constraints this data was not used for developing RFWI, and it was only acquired in some regions.

3.2.5 Wetlands products used for comparison

Besides the VMI national wetland inventory, the wetlands classification (RFWI) developed in this study was compared with another continental, and global wetland maps and inventories. Specifically: ESA WorldCover, the Ramsar Database, LUCAS, MODIS LC1, and GLWD. These datasets are briefly described below, but their backgrounds are described in Section 2.3.

ESA WorldCover LC (Zanaga et al., 2021) (https://worldcover2020.esa.int/download) is

delivered as a 10 m spatial resolution raster (Appendix A Figure A.3). This dataset distinguishes between 11 land cover classes, among which herbaceous wetlands and mangroves can be used to compare with RFWI. Herbaceous wetlands pixels were counted to compute the areas covered by wetlands per county, since in the Swedish territory there were no pixels with the mangroves class.

Ramsar Database contains geographical information of all wetlands in the List of Wetlands of International Importance. It is accessible through the Ramsar Sites Information Service (RSIS), and freely available (https://rsis.ramsar.org/) in vectorial shape, in the form of polygons (Appendix A Figure A.5), and centroid points. The polygons were used to compute the per-county wetlands area.

The LUCAS dataset employed was produced in 2018 (Appendix A Figure A.6), and is freely distributed (https://ec.europa.eu/eurostat/web/lucas/data/primary-data/2018), the latest version (2022) was a work in progress when this study was carried. The amount of land cover classes considered in LUCAS is greater than that of this study and was therefore reclassified into non-wetlands, wetlands, or water, to match the possible outcomes of the RF classifier. The points were employed to extract the class from the RFWI imagery, and the VMI rasterization, for computing a confusion matrix to evaluate the agreement between them. LUCAS comprehends 26,709 field samples taken in Sweden, out of which 3,000 correspond to wetlands (2,465 from inland peatbogs, 533 from inland marshes, and 2 from coastal salt marshes), 207 to inland water, and glaciers, and the remaining 23,506 to other classes. Despite LUCAS points reclassified as wetlands span all counties, they were not evenly distributed, 77% of the samples (2,309 out of 3,000) are located in the three northernmost counties (Jämtland, Västerbotten, and Norrbotten). It should be noted that 2,830 of the 3,000 wetland samples were surveyed from an office, and the remaining 170 sites were visited in the field.

MODIS LC (MCD12Q1) yearly product was acquired (https://developers.google.com/earth-engine/datasets/catalog/MODIS_006_MCD12Q1) to compare wetlands coverage in RFWI with the classification from the Annual International Geosphere-Biosphere Programme (IGBP) (Appendix A Figure A.7). MCD12Q1 LC_type1 product distinguishes 17 land cover classes, including 1 class for permanent wetlands. Thus, similar to LUCAS, it was reclassified to match RWFI classes.

The Global Lakes and Wetlands Database (GLWD-3) developed by Lehner & Döll (2004) is freely available (https://www.worldwildlife.org/publications/global-lakes-and-wetlands-database-lakes-and-wetlands-grid-level-3) for non-commercial, conservation, and educational purposes, and was acquired for comparison with RFWI. The dataset was visually inspected and found to have good accuracy in both the location and extent of many water bodies. However, it contains only five massive wetlands in Sweden (Appendix A Figure A.8).

3.3 Stratified Sampling

Blekinge is the smallest county in Sweden (3,046.02 km^2), and thus able to fit ~30.4 million (10 m) pixels (or points), greatly exceeding GEE classifier thresholds (Section 2.5). Therefore, every pixel falling inside VMI and water polygons can not be used to train, and validate the RF

classifier (Section 2.5), and thus points were sampled within the polygons. 30,000 points per class per county were picked with a stratified random algorithm in GEE, equivalent to 90,000 points per county, and 1,890,000 country-wide. Summing 189 km^2 (0.042%) of Sweden's land area. The amount of 30,000 samples was selected because using 50,000 points did not present any effect on the accuracies, and 50,000 was the maximum possible amount to not trigger errors in GEE. The accuracies and resulting maps for both labeling methods were very stable with 30,000 samples, i.e. the accuracies did not change more than 1% when the randomization seed was changed. This number of samples greatly exceeds those from research found covering large extents, Chen et al. (2017) used 1,184 points for mapping mangroves covering an area smaller than 25,000 ha in southern China. Amani et al. (2019), and Mahdianpari et al. (2020) classified wetlands all over Canada, using 784 km^2 of labeled polygons, and 8,904 reference samples respectively. Hird et al. (2017) used 200 points for classifying, and 40,000 for validation in a 13,700 km^2 region in Canada.

For the ease of the GEE workflow, the points were sampled from a 10 m byte rasterization (matching Sentinel resolution) of the polygons, with a 153,756 x 65,343 shape. 44.78% of its pixels cover Sweden's land and are considered valid. And the raster values could be 0 (no-data), 1 (non-wetlands), 2 (wetlands) or 3 (water). RF is a data-driven algorithm, its sole purpose is training to recognize labels from the inputs. Hence, being the label the most important piece of information, sample labeling was performed in two different ways, for choosing the best performing method.

The labeling method 1 (LM1) starts by rasterizing all of Sweden's land extent, assigning the label to non-wetlands (1), then Översiktskartan polygons are used for changing every overlayed pixel label to water (3), and finally, VMI is used to assign wetlands label (2) to every pixel it overlays (Figure 6, left). Hence, all of the valid (land) pixels have a class, 82.26% (370,121 km^2) belonging to non-wetlands, and the remaining 9.59% (43,161 km^2), and 8.15% (36,662 km^2) to wetland, and water pixels, respectively. The changes in areal coverage per class due to the rasterization are assumed to be negligible. This method is easy to implement, and points are widespread in the counties (Figure 7a), but wetlands are sampled directly from VMI, introducing the challenge of explaining disagreement between VMI and RFWI (new national wetlands inventory). i.e. Disagreement could be due to the classifier not capturing the underlying phenomena, and failing to properly classify the features on the ground. Or due to actual changes in land cover that happened after VMI was surveyed, that the trained classifier successfully mapped. Moreover, with this labeling method some samples might mislead the classifier, a fraction of non-wetland samples can be wetlands in reality, since VMI does not include every wetland (Section 2.4), additionally, wetlands from VMI could have disappeared, labeling non-wetlands as wetlands.

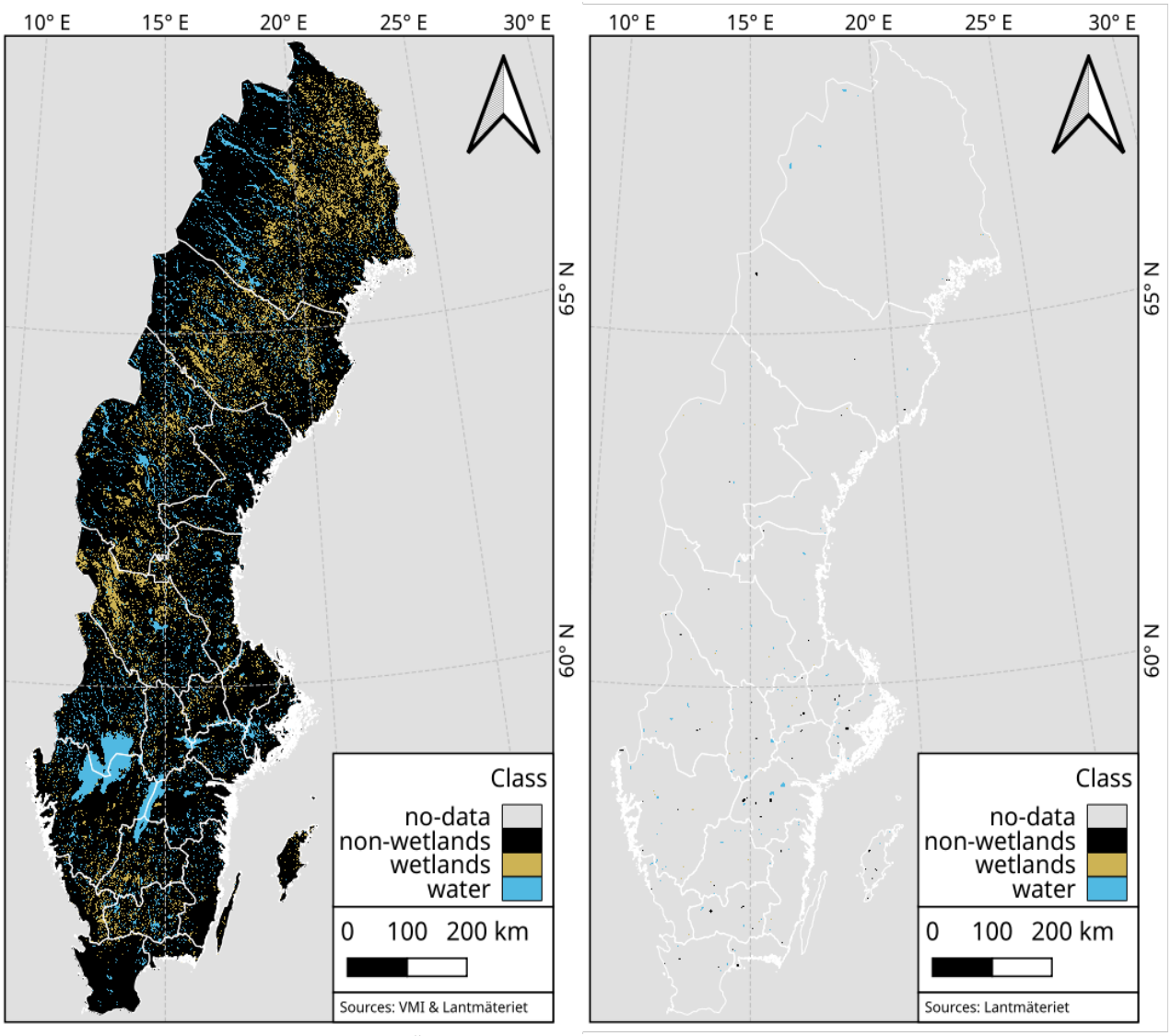

***Figure 6**. Rasterized version of VMI and Översiktskartan polygons for labeling method 1 (left) and rasterization of digitized polygons for labeling method 2 (right).*

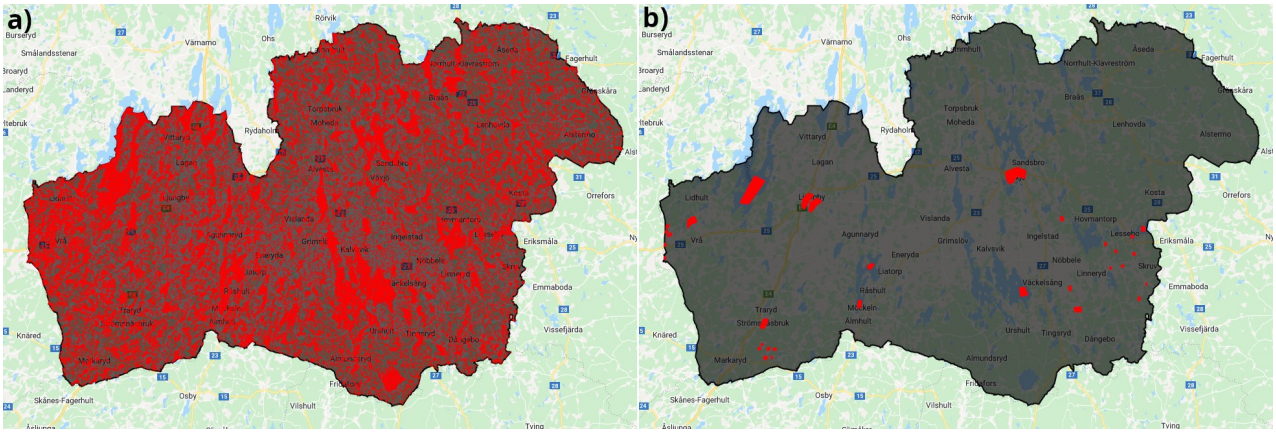

***Figure 7**. Example of sampled points (red dots) with LM1 (a), and LM2 (b), in Kronoberg (black outline).*

The labeling method 2 (LM2) was performed to address the intrinsic uncertainty of LM1. LM2 in short was restricting where the points could be sampled from, by digitizing new polygons.

Google Earth satellite imagery was employed as a base-map for overlaying VMI & Översiktskartan polygons. New polygons for the wetlands, and water classes were drawn within VMI's (Figure 8), and Översiktskartan's polygons, respectively. Inside most of VMI's wetlands (e.g. Figure 8), a brownish color (with green tint in occasions), and even texture without apparent vegetation was found to be the rule in Google Earth satellite imagery, and helped drawing the new polygons. Only in exceptional cases wetland polygons were drawn outside VMI's polygons, specially in the north, where Google Earth's imagery had low quality. Digitization of non-wetlands was performed as an effort to capture reflectances not attributable to wetlands or water, ensuring to not overlap those classes, but spanning multiple other LC, e.g. agricultural, built-up, forests, among others. LM2 reduces uncertainty by assuring the quality of the labels feeding the classifier, corroborating that no point within one class could represent another class. Nevertheless, hand-picking features is extremely time-consuming and reliant on visual interpretation. To address the spatial variation of vast areas, polygons were digitized as sparsely as possible (Figure 7b). In contrast to LM1, LM2 greatly reduces the number of valid pixels within a class (Figure 6, right), due to the effort required in digitization. E.g. Sweden's inland is represented by a 100% of valid pixels, those belonging to non-wetlands, wetlands, and water classes cover 0.083% (373 km^2), 0.028% (124 km^2), 0.137% (615 km^2), respectively, summing up 1,112.79 km^2 of digitized area. Table 3 summarizes the digitized (for LM2) and total areas of every county.

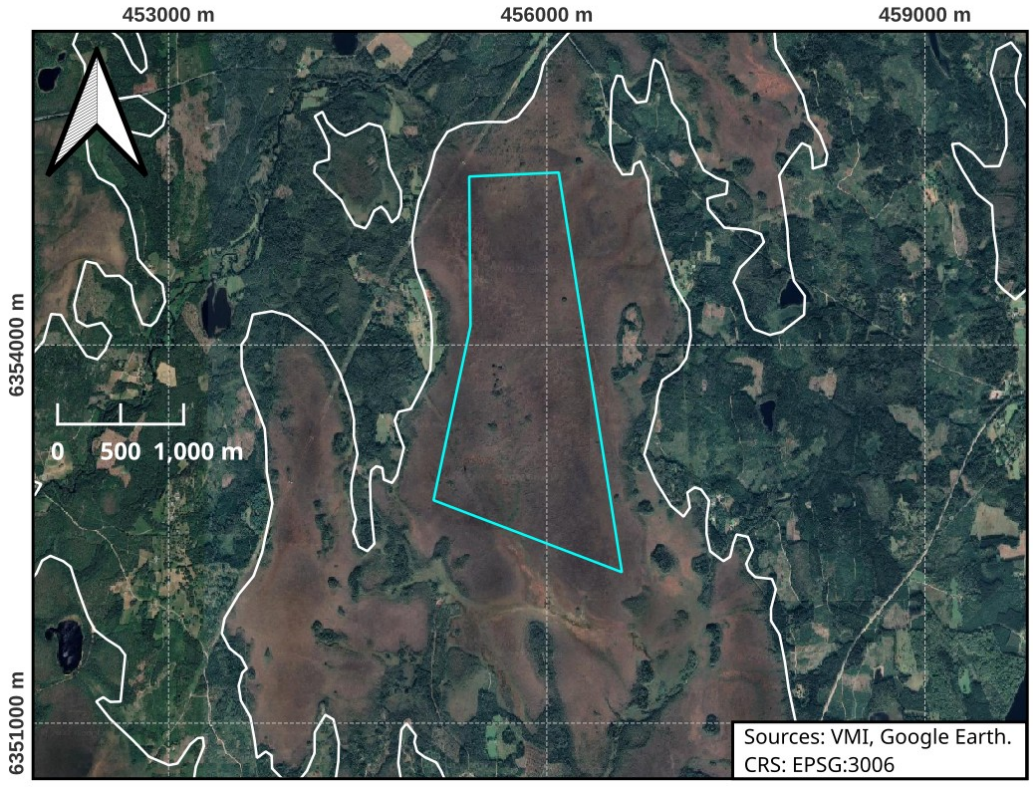

***Figure 8**. Example of a digitized polygon, Kronoberg's county. VMI in white outline, and a digitized polygon for LM2 in cyan outline.*

During the digitization, disagreement between the satellite imagery and VMI polygons was found, confirming the uncertainty attached to LM1. Many wetlands are outside VMI polygons,

and many wetlands were not surveyed in VMI e.g. *Fäjemyr,* a 310.5 ha well documented, and relatively untouched wetland (Länsstyrelsen Skåne, 2016), located in Hässleholm, Skåne, is not included in VMI (Figure 9). Figure 10 shows the high water table and inundated vegetation of Fäjemyr in September 2021. Also, VMI polygons' boundaries are very smooth, do not delineate wetlands correctly, and span non-wetland land cover classes like forests, agricultural lands, and water.

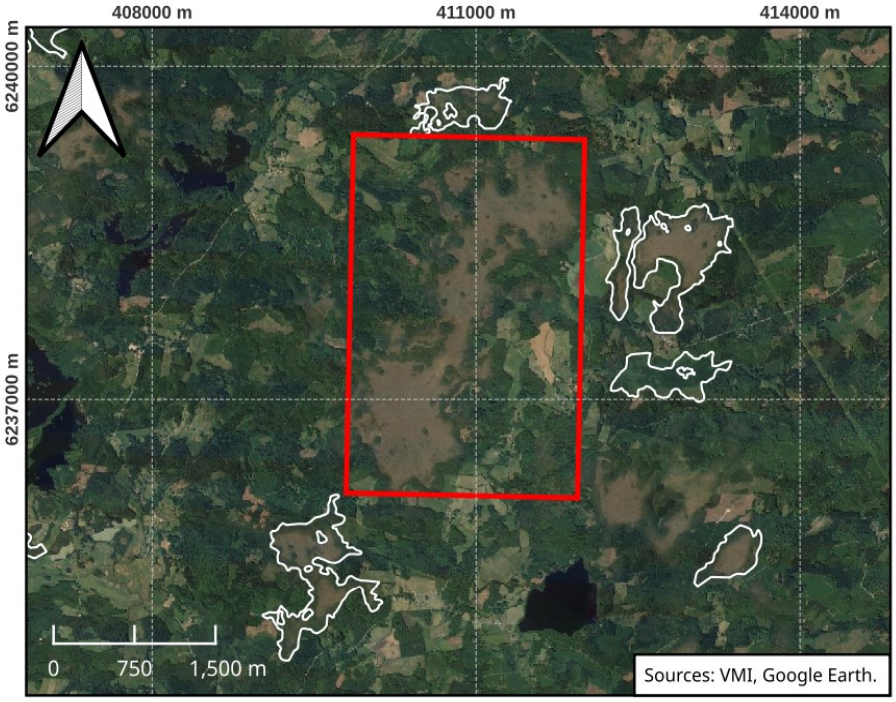

***Figure 9**. Fäjemyr wetland inside the red rectangle, VMI polygons in white outlines.*

***Figure 10**. Fäjemyr's high water table, sedges, lichen, and moss (Own). Photograph captured in September 2021 on a field trip to Fäjemyr.*

LM1 points are restricted to a distance of 100 m from one another, accounting for the spatial variability of every county's vast area (Hird et al., 2017). While for LM2 points are separated 10 m from one another, ensuring points never sample the same pixel (Figure 11).

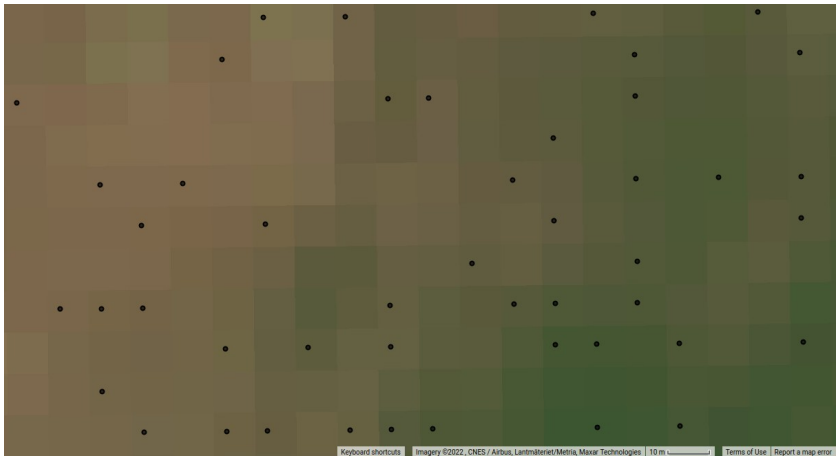

Figure 11. *Example of pixels sampled into points.*

3.4 Training

The Random Forest (RF) algorithm was adopted in this study to classify the inputs on a pixel-wise basis. The training and validation of the classifier were performed in each county, with points sampled within the boundaries of each county. Most of the workflow, before the interpretation of the classified imagery, was performed in the GEE environment.

Amani, Mahdavi, et al. (2019) used 80 trees, and a minimum leaf population equal to 2, as the optimal parameters for a big extent such as an entire Canadian county, while Mahdianpari et al. (2020) used 500 trees. Both authors coincide with the remaining GEE classifier's defaults (Google, n.d.-b), setting the fraction of input to bag per tree to 0.5, and the number of variables per split to be the square root of the number of variables. Multiple sets of RF parameters were tested during this study. The selection of the number of trees was based on the fact that using 200 or more trees did not improve the accuracies. 500 trees were too intensive for the dimensionality of the inputs, many counties ended in *user memory exceeded* errors, and computing time incremented drastically for the counties that could be classified successfully. 20 trees diminished the accuracies by around 1-2 % when compared to 80 trees. And thus 80 trees were chosen due that Random Forest can not over-fit the data by increasing the number of trees, and using more than required is not detrimental (Breiman, 2001; Mahdianpari et al., 2020; Rana & Venkata Suryanarayana, 2020). Increasing the minimum leaf population up to 60, instead of 1 (default), did not influence the accuracies, thus it was left unchanged. Similarly, bagging fraction values between 0.1 and 0.9 were tested, and variations in the accuracies did not exceed 1%, thus the default (0.5) was preferred. After thorough experimentation with the parameters, major changes in the accuracies were not found.

The general observation after the hyper-parameter tuning (testing of different parameters) is that the RF algorithm is highly dependent on the input data, and very stable regardless of the parameters used. It is worth mentioning that the hyper-parameter tuning was performed with the evaluation subset obtained from LM1.

Therefore, the same parameters were used for every RF classifier: 80 trees, 4 variables per split (rounded-up square root of the number of variables), 1 sample minimum leaf population (minimum number of points for creating nodes), a bagging fraction equal to 0.5 (or 50% the training set), and no limit of nodes (max nodes set to null). All of the parameters besides the number of trees are Google Earth Engine's defaults. The selection of the classifier's parameters was a combination of research review, and observations from the hyper-parameter tuning.

The multi-source multi-temporal data fused with the labels is considered ready for training a ML classifier after being flattened as a data frame or feature collection (a table structure), where every row (observation) is a different pixel or point, and each column or variable (attribute) is a different band or index. Each row has 14 columns, that include 1 target band (label input classes), 6 from Sentinel-2 (4 bands plus 2 indices), 2 from Sentinel-1 bands, and 3 from topographic data.

One classifier was trained for each county, in accordance to what have been found to work best in great extents (Amani, Mahdavi, et al., 2019; Mahdianpari et al., 2019). Of the 90 thousand points sampled per county, 54 thousand (60%) were used for the training step, and the remaining 36 thousand (40%) were reserved for validation. Thus, each 10 m pixel covers 100 m^2, and the effective area of each state sampled, for training, and validation sets are 5.4 km^2, and 3.6 km^2 county-wise, respectively.

3.5 Accuracy assessment with reference samples

After training a classifier, a Confusion Matrix can be computed, measuring agreement by comparing the label of the points used for training, and the class they are predicted to have. An Error Matrix can be subsequently computed, by classifying the validation set and comparing it to their labels. From the matrices, the overall (OA), user's, and producer's accuracies, and kappa coefficient are calculated using Equations Error: Reference source not found-Error: Reference source not found. A classifier was trained for each county, for both labeling methods, thus the per county accuracy of both labeling methods could be assessed.

$$\text{Overall Accuracy} = \frac{\text{Number of correctly classified sites}}{\text{Total number of reference sites}} \tag{6}$$

$$\text{Class User's Accuracy} = \frac{\text{Class' number of correctly classified sites}}{\text{Class' total number of reference sites}} \tag{7}$$

$$\text{Class Producer's Accuracy} = \frac{\text{Class' number of correctly classified sites}}{\text{Class' total number of classified sites}} \tag{8}$$

$$q = \frac{\text{The sum of class-wise products of total classified and reference sites}}{\text{Total number of correctly classified sites}}$$

$$\text{Kappa Coefficient} = \frac{\text{Sum of correctly classified sites} - q}{\text{Total number of classified sites} - q} \tag{9}$$

In equations 6-9 q is the class-wise product between total classified and reference sites divided by the total number of correctly classified sites.

3.6 Comparison of RFWI and other wetlands products

The reclassified LUCAS points were used to extract the class from the classified imagery, and used later as reference sites in an Error Matrix, to measure the agreement with RFWI.

The per county areal coverage of wetlands in RFWI is computed by counting the pixels of the classified imagery, from a classifier trained with the set LM2 (further developed in Section 4.1). The same process was performed with the sets sampled with LM1. The areas classified as wetlands in both RFWI, and with the LM1 classifier, were compared against VMI, ESA WorldCover, Ramsar Database, and MODIS global LC1 product, in terms of county-wise wetlands area. Visual inspection was also performed, to assess the underlying reasons of differences.

4 Results

4.1 Wetlands classification and accuracy assessment

Using the sampling method LM1 did not perform well as it considerably wrongly classified non-wetlands as wetlands, leading to a large overestimation of wetlands occurrence. Using LM2 it was possible to achieve much better results, and thus it was used for the generation of the final wetland classification method (RFWI) in this study. It should be noted that any result reported as of RFWI hereafter is a product of a classifier trained using LM2 samples. The overall accuracy (OA) of the classified validation set (LM2) is 98.97%, with a Kappa value of 0.985, where the county with the maximum overall accuracy (99.84%) was Kronoberg, while Norrbotten presented the minimum (97.40%). Both user's, and producer's accuracies are 98.97%, with a Kappa value of 0.999. The accuracies and kappa coefficients of LM2 on a per-county basis are presented in Table B.1. The accuracies for LM1 can be found in Table B.2. Figure 12 (left) illustrates the new Sweden's countrywide wetlands inventory (RFWI), produced by classifying the aforementioned inputs with LM2, using the RF algorithm, alongside VMI for comparison. A full-page RFWI map is in Appendix A Figure A.9.

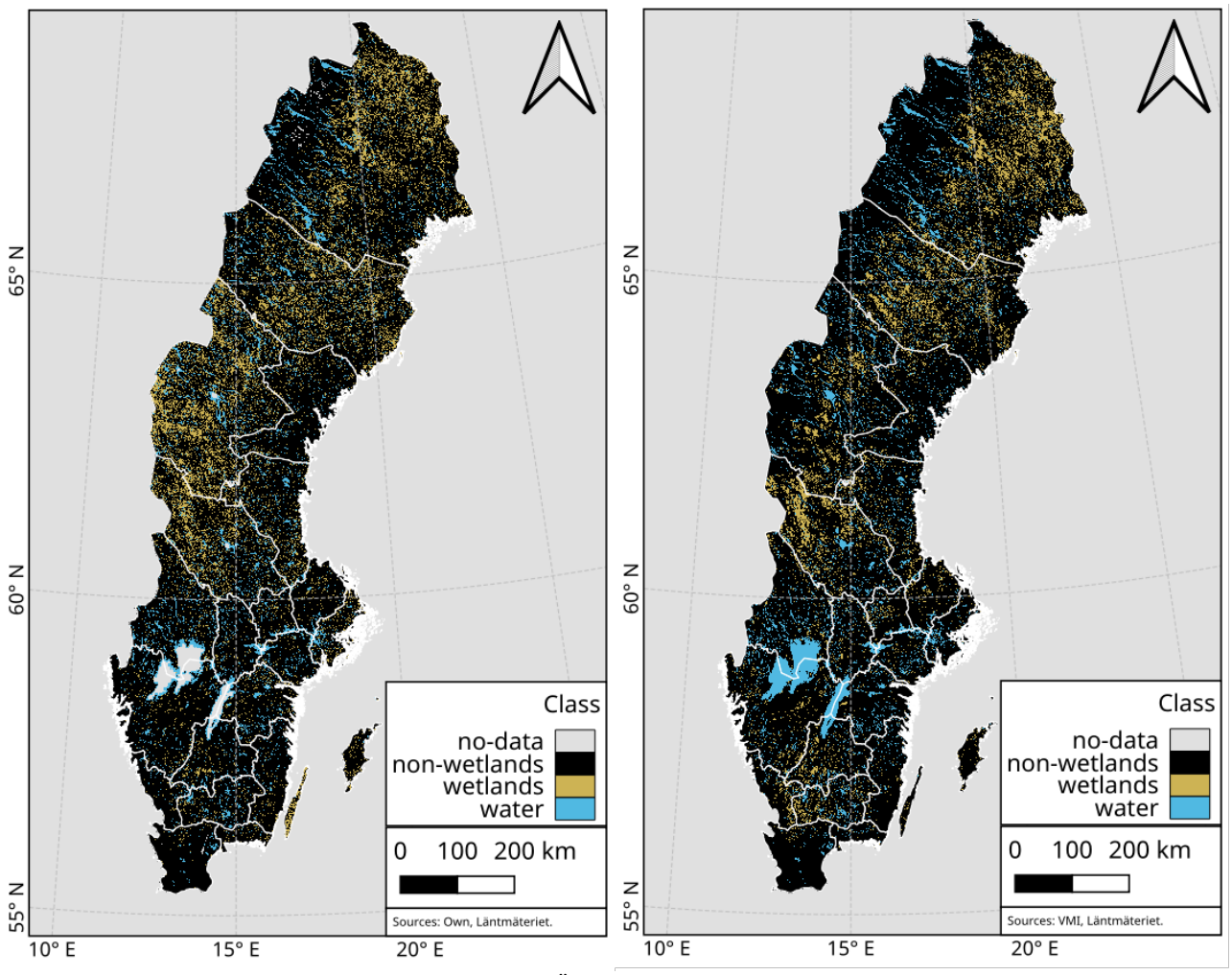

***Figure 12**. RFWI (Left) and rasterization of VMI and Översiktskartan polygons (Right).*

The agreement between RFWI and VMI can be found visually. Western Dalarna, and striped regions in Västerbotten, and Norrbotten seem to contain the most wetlands in both. But RFWI seem to overestimate wetlands occurrence in Stockholm, Öland (Kalmar's), and Jämtland.

The normalized feature importance computed during the classifications indicates what inputs improved accuracies the most, displaying an appreciable pattern (Figure 13). Topographical and radar data were the most beneficial, and optical data presents the lowest values. Nevertheless, the Y-axis must be considered, and while the importance seems to be correlated with the data source, the contribution of optical imagery was not negligible. The best- and worst-performing features are TWI, and B4, with values of 9.51% and 8.67%, respectively.

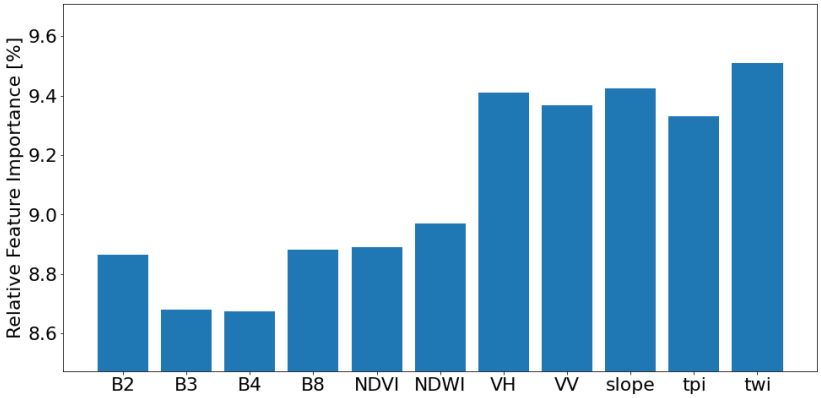

***Figure 13**. Random Forest's Feature Importance, county-wise sum.*

4.2 Comparison of RFWI and VMI

The areal coverage of wetlands in RFWI exceeds that of VMI by 30.88% at the national scale (Table 4), as expected due to VMI limitations (Sections 2.4). But the difference in wetlands coverage is not evenly distributed across the country. In 6 counties the area classified as wetlands in RFWI is smaller than in VMI (Jönköping, Kronoberg, Halland, Västra Götaland, Örebro & Västmanland), with differences ranging 25-73%, being Halland the county with the biggest reduction in wetlands area. In the remaining counties the area classified as wetland in RFWI is bigger than what was surveyed in VMI, in 7 counties (Uppsala, Södermanland, Gotland, Skåne, Dalarna, Västerbotten & Norrbotten) the increment is small (less than 30%), 4 counties (Blekinge, Värmland, Gävleborg & Västernorrland) show a mild increase (between 38-64%), 3 of the 4 remaining counties (Östergötland, Kalmar & Jämtland) showed a high percentual difference in wetlands area (between 202-245%), and Stockholm showed the greatest percentual increment (451%). Table 4 also shows the area classified as wetlands when using a classifier trained with the training subset from LM1, which shows increments ranging 73-975% compared to VMI values, and none of the counties are estimated to have smaller areas than VMI with LM1. Additionally, ESA WorldCover, MODIS, and Ramsar data are presented in Table 4 for comparison.

Halland in RFWI has an area equivalent to 27% of VMI's, suggesting that a great loss in wetlands coverage may occurred in the county. This change is visually appreciable (Figure 14), VMI polygons greatly overestimate the occurrence of wetlands in the county by two means,

enclosing extents where wetlands are no longer present, or exaggerating their size. i.e. a shrinkage or destruction of the sites surveyed in VMI.

***Table 4**. Wetlands areal coverage [km^2] according to different sources.*

County	VMI	RFWI	LM1	WorldCover	MODIS	Ramsar
Stockholm	147.85	814.54	1,347.04	47.35	299.77	152.00
Uppsala	424.17	430.24	2,042.52	87.80	88.16	176.84
Södermanland	236.29	270.14	1,435.50	53.84	134.63	122.58
Östergötland	262.48	794.58	2,356.31	51.87	109.36	130.68
Jönköping	1,154.78	521.03	2,541.03	158.95	23.20	151.94
Kronoberg	1,001.38	440.68	2,245.30	84.21	51.92	328.33
Kalmar	303.31	1,047.65	3,100.05	65.94	101.28	141.08
Gotland	243.41	312.22	955.66	41.47	78.52	66.08
Blekinge	166.64	230.77	757.97	8.56	36.52	155.27
Skåne	114.37	148.51	1,229.87	48.88	111.50	235.06
Halland	593.00	160.36	1,343.94	26.97	33.54	156.26
Västra Götaland	1,271.63	882.92	5,243.34	228.10	265.26	323.47
Värmland	765.92	1,193.49	3,915.73	220.44	102.57	90.53
Örebro	412.01	312.57	1,877.30	103.85	55.31	66.57
Västmanland	658.24	313.10	1,313.09	51.02	77.11	337.46
Dalarna	5,366.40	5,849.08	8,676.06	228.95	61.92	356.13
Gävleborg	1,364.73	2,167.04	4,347.55	117.13	89.73	192.49
Västernorrland	793.97	1,300.05	4,525.66	90.16	125.37	48.89
Jämtland	4,496.18	13,788.05	10,800.85	272.69	368.66	494.89
Västerbotten	8,274.98	9,973.56	15,167.36	563.59	324.58	1,917.12
Norrbotten	15,139.90	15,580.59	26,243.00	2,443.20	1,185.13	2,493.18
Sweden	**43,191.64**	**56,531.17**	**101,465.14**	**4,994.95**	**3,724.02**	**8,136.85**

Fäjemyr's example provided during Section 3.3 was properly mapped in RFWI (Figure 15, pink outline), and its boundaries were clearly delineated. The classification product from the classifier trained with points from LM1 (Figure 15c) is shown to highlight the overestimation of wetlands in the region. Other new wetlands were identified close to Fäjemyr, and some surveyed in VMI disappeared (green outline in Figure 15).

Stockholm has the biggest percentual change between RFWI, and VMI (451% or 666.69 km^2). The increase is not realistic (Figure 16), since many pixels that apparently cover urban, forest, or cropland land cover are classified as wetlands. But Jämtland has the biggest areal difference (9,291.87 km^2 or 200%) between RFWI, and VMI, accounting for nearly 70% of all the country-wide differences in wetlands area between both. Figures 16 & 17 show a wetlands overestimation in RFWI (d), and LM1 (c), compared to VMI (b), in Stockholm and Jämtland, respectively.

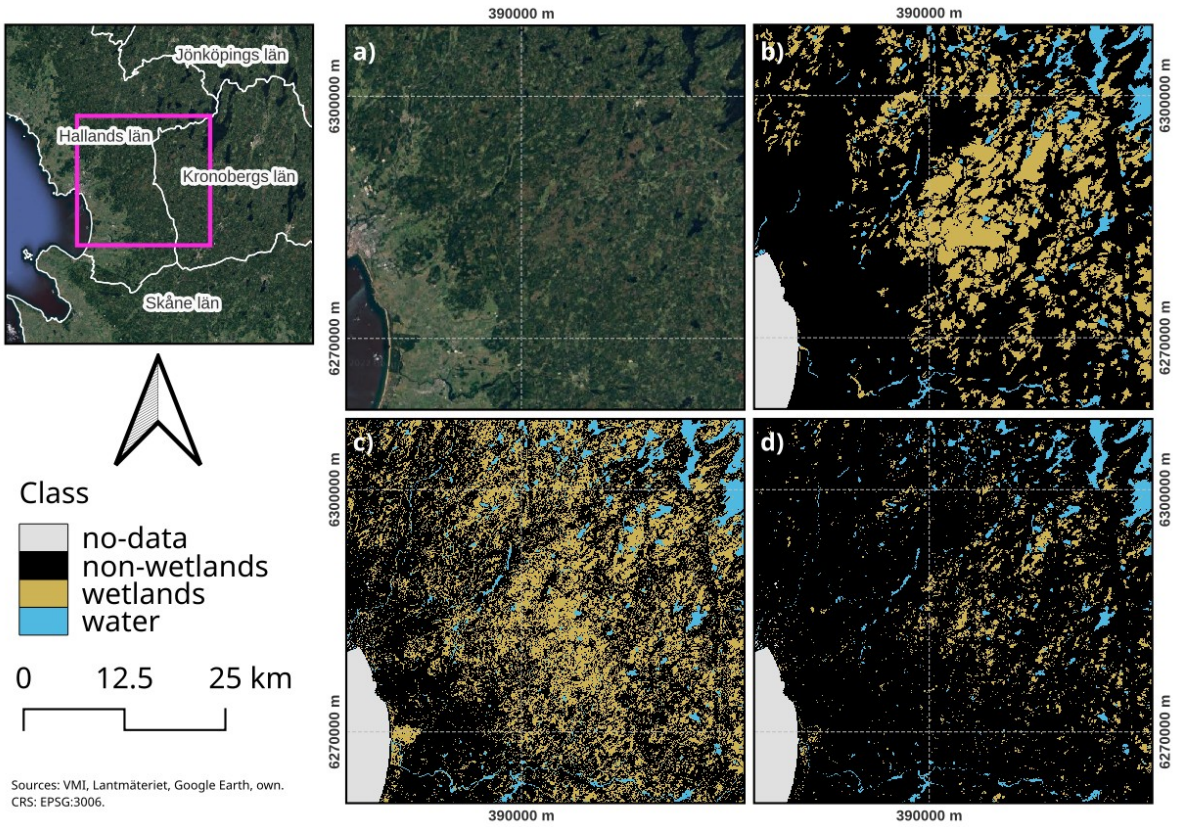

Figure 14. *Zoomed-in Halland map. Google Earth (a), VMI (b), LM1 classification (c), RFWI (d).*

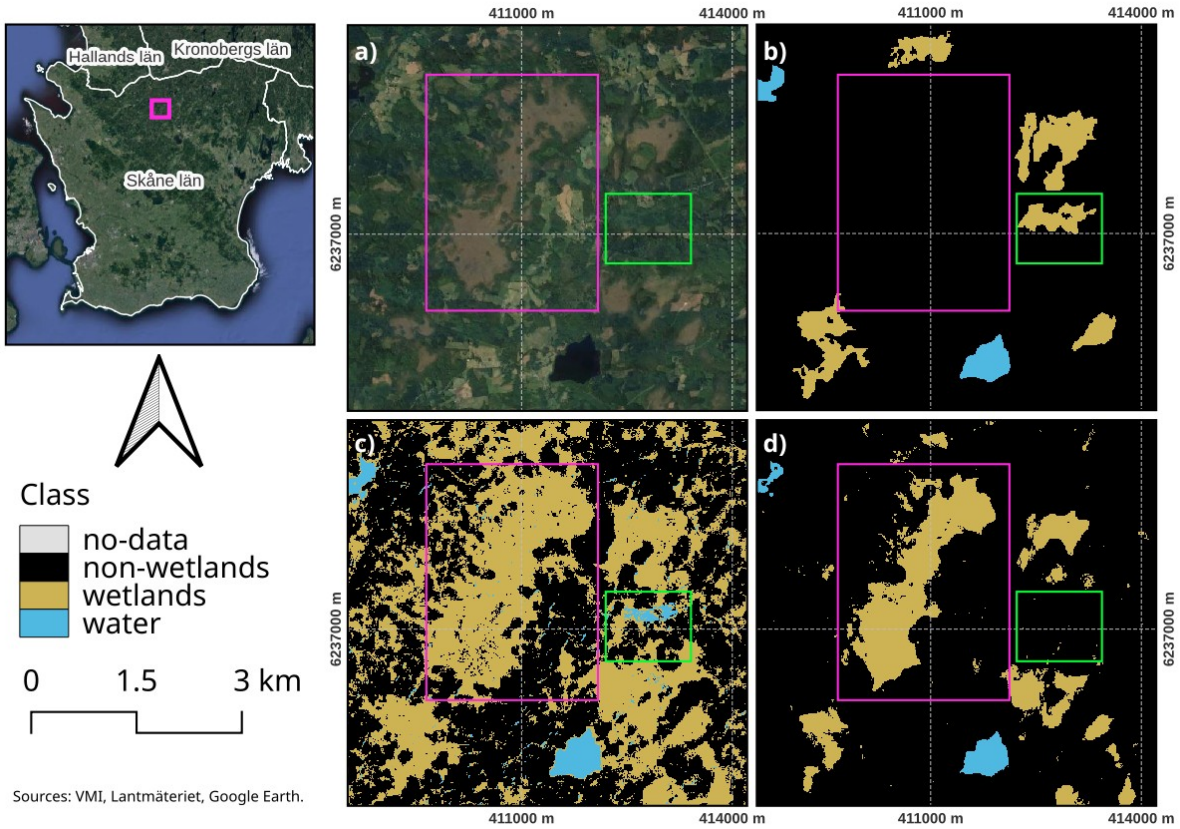

Figure 15. *Skåne zoomed-in map. Google Earth (a), VMI (b), LM1 classification (c), RFWI (d). Fäjemyr wetland inside a pink outline, and a wetland lost since VMI survey highlighted in green.*

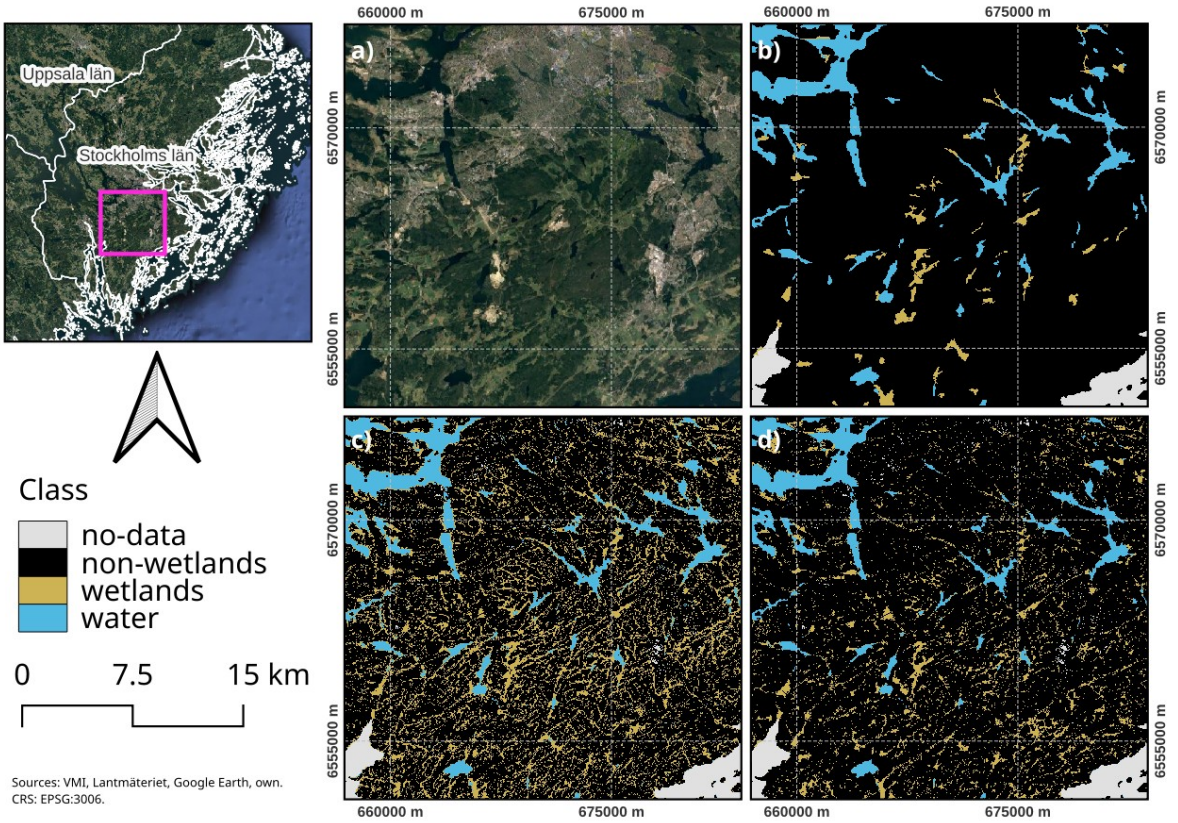

***Figure 16**. Zoomed-in Stockholm map. Google Earth (a), VMI (b), LM1 classification (c), RFWI (d).*

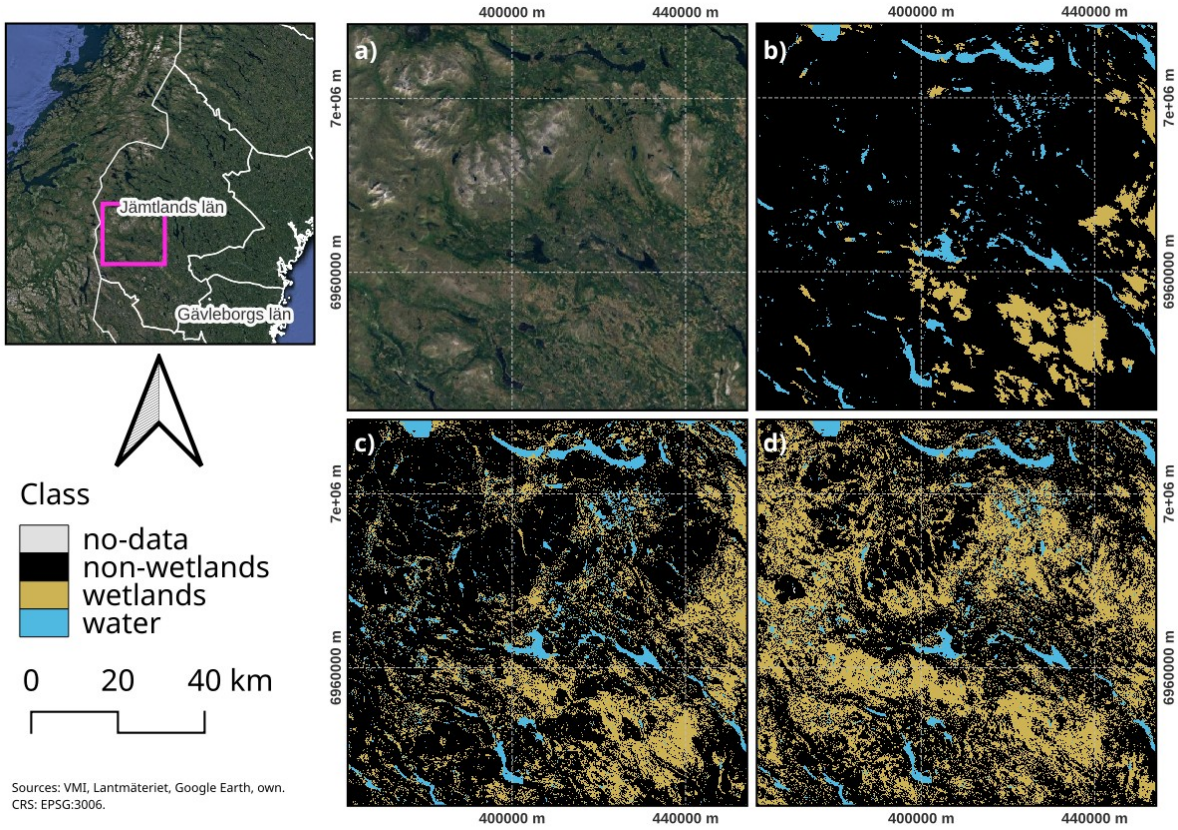

***Figure 17**. Zoomed-in Jämtland map. Google Earth (a), VMI (b), LM1 classification (c), RFWI (d).*

Two tests were carried out to assess how higher resolution topographical data can affect the

results. The same classifiers used for RFWI in Stockholm, and Jämtland, were used to classify the data in a small region within each state, but using the national DEM Grid 2+ topographical data instead of Grid 50+ (~2 m spatial resolution instead of ~50 m). This test was performed in two of the regions where the biggest difference in areal coverages between RFWI, and VMI was found. Figure 18 illustrates great differences found in the two afar regions (Stockholm in Figure 18a & Figure 18b, Jämtland in Figure 18c & Figure 18d), by training the classifiers from the same Grid 50+ data, but classified from differing datasets (Grid 50+ for Figure 18a & Figure 18c, and Grid 2+ for Figure 18b & Figure 18d). The difference in wetlands' areal coverage, in the aforementioned regions, is more than 50%. The wetlands area in Figure 18a (RFWI , Stockholm) is 75.08 km^2, in Figure 18b (Grid 2+, Stockholm) is 18.46 km^2, in Figure 18c (RFWI, Jämtland) is 550.31 km^2, and in Figure 18d (Grid 2+, Jämtland) is 235.14 km^2.

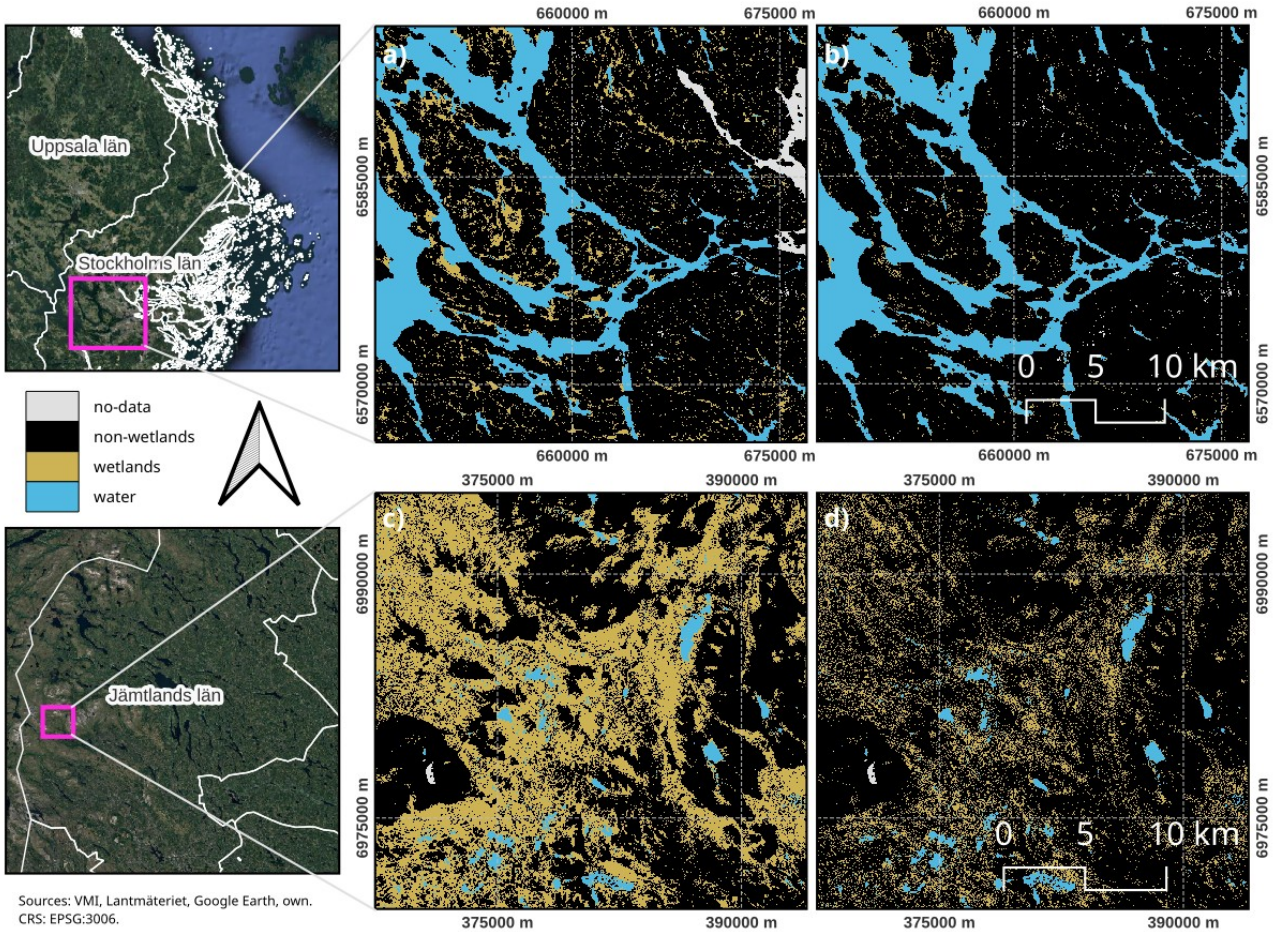

***Figure 18**. Zoomed-in classification maps in Stockholm (a & b), and Jämtland (c & d). RFWI (classified with GSD 50+ data) on the left (a & c). Classifications with GSD 2+ data on the right (b & d).*

A extent of 5,398.09 km^2 (approximately 1.12% of Sweden's land) does not have a class assigned in RFWI, due to masked, and no-data pixels used as input for prediction.

4.3 Comparison of RFWI and other wetlands products

All of the Global LC products acquired for comparison (ESA WorldCover, MODIS LC1, the GLWD-3, and the Ramsar Database) report wetlands areas much lower than what was classified

in RFWI, and what was surveyed in VMI (Table 4).

ESA WorldCover (Appendix A Figure A.3) product wetlands cover (4,994.95 km^2) less than 9% of the country-wide area classified as wetlands in RFWI (56,531.17 km^2) and 11.5% of the area surveyed as wetlands during VMI (43,191.64 km^2). The fractions are very small, hence ESA WorldCover product is under-estimating the occurrence of wetlands in Sweden.

MODIS LC1 product (Appendix A Figure A.7) also presents a very small fraction (3,724.02 km^2) of the wetlands classified in RFWI (6.6%), and surveyed in VMI (8.6%). This product only includes wetlands in the water-land interface.

The Ramsar Database (Appendix A Figure A.5) country-wide area (8,136.85 km^2) approaches 15% of RFWI's wetlands area, and is close to 19% of VMI's area. The Ramsar Database includes a whole watercourse located in Västerbotten, not surveyed in VMI, and classified as water in RFWI. This feature was inspected against satellite imagery in Google Earth, and it appears to be an error in the Ramsar Database, causing a likely over-estimation of wetlands in the county.

GLDW-3 (Appendix A Figure A.Error: Reference source not found) was not utilizable because it only contains wetlands in four counties.

The confusion matrix (Table 5) generated with LUCAS points as reference sites, and the RFWI class at their location indicates an 87.88% OA, with a 0.497 kappa coefficient. While the OA is very good, the kappa coefficient indicates that the results are not entirely trustworthy, specially for the wetlands. The location of the wrongly classified points does not visually show any spatial distribution, and seems evenly distributed along the country. Table 5 shows that 2,063 points surveyed during LUCAS as non-wetlands, are classified as wetlands in RFWI. 80% of these misclassified points belong to the woodlands, grasslands, or shrublands classes. On the other hand, 1,037 points surveyed as wetlands in LUCAS, are classified as non-wetlands in RFWI. Many of these misclassified points were visually found to neighbor pixels classified as wetlands.

Table 5*. Confusion Matrix for LUCAS as reference sites, and RFWI as classified. Classes: No-Data (ND), Non-Wetlands (NW), Wetlands (We), Water (Wa).*

		RFWI					
	Class	ND	NW	We	Wa	Total Row	Producer's Accuracy
LUCAS	ND	0	0	0	0	0	0
	NW	26	21,414	2,063	3	23,506	91.10%
	We	0	1,037	1,961	2	3,000	65.37%
	Wa	25	65	15	98	203	48.28%
	Total Column	51	22,516	4,039	103		
	User's Accuracy	0	95.11%	48.55%	95.15%		

5 Discussions

5.1 Unfruitful preliminary tests

As part of the initial testing of multiple inputs, various sets of inputs were discarded in the process, this chapter's section explains what (and why) some data was discarded.

Initially, three seasonal images from the multi-temporal collections (optical, and radar data) were computed for each band, and index, covering 3-month periods, more specifically for spring (March, April & May), summer (June, July & August), and fall (September, October & November) seasons. Winter was quickly discarded due to a vast amount of snowy pixels. Interestingly, the other seasons ranked similarly in the feature importance, being the data source (optical, radar, or topographical) the major cause of variation behind feature importance. Spring was like winter presenting a high amount of snowy pixels, causing no-data due to the threshold set on band 1, specially in the northern counties. And finally, including Fall season imagery among the inputs was not improving the accuracies by more than 1% in most counties, being discarded as well. It is therefore assumed that a very high correlation exists between seasons.

Three additional bands in the VIS-NIR meant for monitoring vegetation (European Space Agency, 2015), were also tested as input for different counties, B5: 704±7.5 nm, B6: 740.5±7.5 nm, and B7: 782.8±10 nm. Their contribution was negligible, ranking similarly between each other in the feature importance, always among the 5 worst-performing. Therefore, they were discarded.

The Normalized Difference Polarization Index (NDPI) was also computed and added as an input during preliminary tests, but discarded due to the degradation of the resulting classification by introducing a salt and pepper type of random noise i.e. having wetlands and non-wetlands pixels mixed in large extents, similar to the look of throwing salt and pepper over an image. Intrinsically incorrect since land-cover classes are not expected to change every 10 meters, but encompass larger extents in a more contiguous manner. NDPI is used to enhance the differences between VV and VH bands, similar to NDVI & NDWI with VIS bands. And it has been employed in other studies because it contains roughness and textural information (Hird et al., 2017; Yun-gang et al., 2008), can help mapping soil moisture (Hird et al., 2017), and is successful for predicting landslides in inundated soils (Yun-gang et al., 2008). However, it was not found beneficial.

Employing the elevation values directly from the DEM as an input, was tested and discarded due to a negative impact in the classifications, not appreciable in the accuracies but found during visual interpretation. More specifically created a segmented distribution of the wetlands class, where most of the cells classified as wetlands would be found away from coasts, even in counties (e.g. Gotland, Stockholm) where a great amount of coastal area is covered by wetlands.

5.2 Discussion of results

The county-wise wetlands areas are very similar between VMI and RFWI, nevertheless they are greater in 15 out of 21 counties. Excluding Stockholm and Jämtland, the wetlands area is greater

in RFWI than in VMI because it captures finer scale details in many of the wetlands, and RFWI contains many smaller wetlands not surveyed in VMI. Figure 15 shows the ability of a single classifier (trained and predicting with data from Skåne) to classify new areas as wetlands, and also detect lost wetlands. This phenomenon is observed in every county. A huge portion (~70%) of the country-wide wetlands areal difference between RFWI and VMI (13,339 km^2) is found in Jämtland (9,291 km^2), the increment does not appear entirely unfounded since many areas classified as wetlands in the county appear in Google Earth similar to those used for labeling. But this result certainly includes an overestimation of the wetlands occurrence; forests and other types of landcovers' pixels were classified as wetlands due to labeling related issues. The difficulty of drawing polygons in this county might be the culprit, since points within the boundaries of some digitized polygons can be of landcovers neighboring wetlands, hindering the ability of the classifier to distinguish classes.

The fact that one classifier was trained for every county, with labels from within the county's boundaries, might be thought of as counter-intuitive, and constraining the possibility of extrapolation. Thus, there are reasons supporting this decision. Figure 19 illustrates an example of the country-wide distribution of the data, from one of each data source (optical, radar, and topographical), but separated for each labeling method and class. It shows how the data, and signature reflectances between classes overlap. Not even for the input with the best relative feature importance (TWI), an easy separation is plausible on a country-wide scale with only one variable. The data from wetlands sampled with LM2 shows differences between counties, in the means, quartiles, and overall distribution. An example of this phenomenon is illustrated in Figure 20, in the VV, and TWI bands. This supposes that a single classifier for the whole country or training with samples from multiple counties might not be ideal. This reasoning might be further supported by the overall worse accuracies, and wetlands overestimation of models trained with samples from LM1, which present a much more similar behavior between counties (Figure 21).

The high accuracies are attributed to the combination of multi-source imagery, based on the assumption that the response from on-the-ground bodies to EM radiation in different bands, will vary depending on the intrinsically different characteristics of each object. Nevertheless, the accuracies are much higher than those reported by similar research, three reasons were discussed to explain these results:

1. The points in LM2 (used for RFWI) are very close to each other and due to spatial correlation the sampled values (neighboring pixels) will be similar, more than those sampled in LM1. High spatial autocorrelation between the training and validation datasets can lead to over-optimistic OA (Ploton et al., 2020). Nonetheless, LM1 accuracies are still very competitive when compared to the similar research, pointing out that this might not be the only reason.

2. For the whole argument supporting this study, we are assuming that the ML algorithm can pick, and distinguish the same patterns that humans are capable of. Besides the similarities that exist between LM2 points within a class in the same county, it is important to stress they were sampled from polygons digitized by visual interpretation, of Google Earth's satellite

imagery true color composites. Therefore, it is not surprising that the algorithm, disposing of more data than the human interpreter, can correctly classify the points, resulting in ~99% accuracies.

3. This study is separating only three classes (water, wetlands, and other areas); this is a much simpler task for a classifier than separating marshes, bogs, swamps, and other wetland types. Authors that reported lower accuracies usually employed ground truth that distinguish between wetlands types, and separate non-wetlands into urban, forests, grasslands, and croplands (Amani, Mahdavi, et al., 2019; Berhane et al., 2018; Mahdianpari et al., 2019; Tian et al., 2016). The introduction of additional classes can diminish the OA, due to similar reflectances among wetland types (Amani, Mahdavi, et al., 2019).

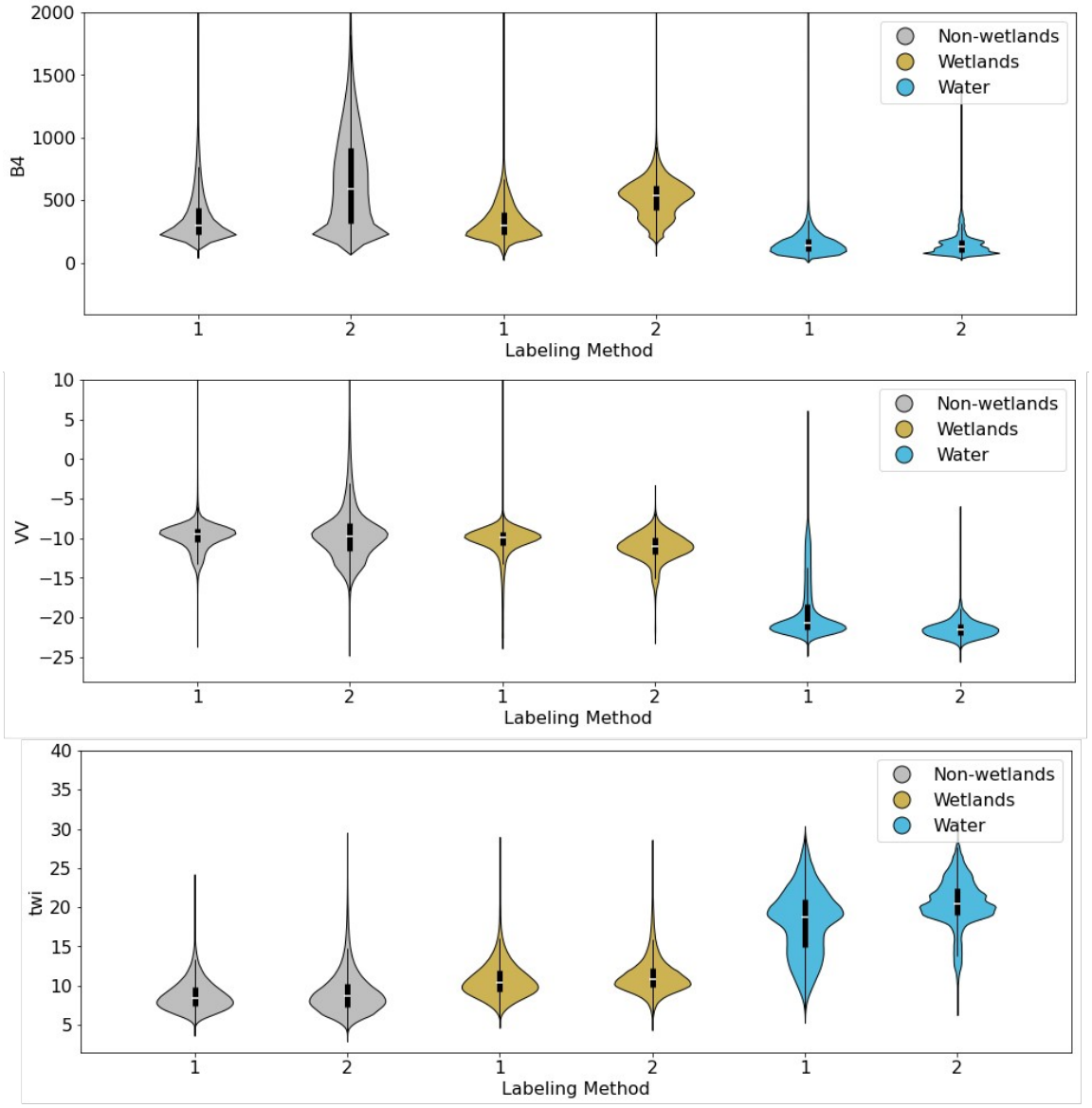

***Figure 19**. Violin plots containing a dimension of each data input source (B4 from optical, VV from radar, and TWI from topographical), per class, per labeling method. The white line represents the median, the thick black line the interquartile range, and the thin black line the confidence interval.*

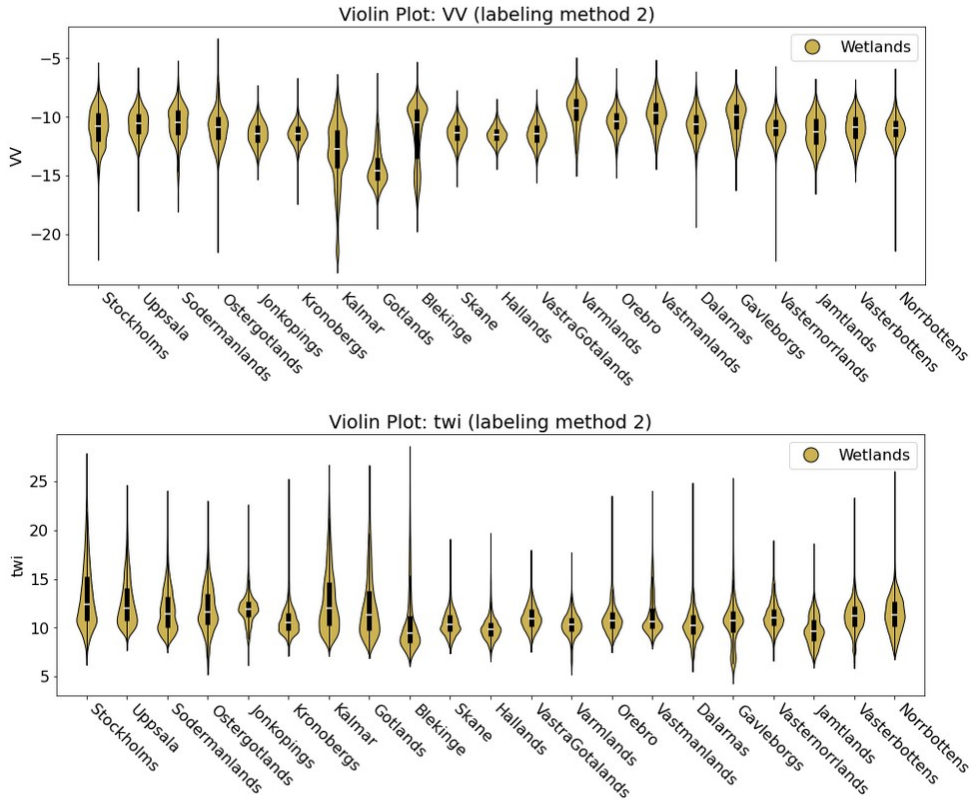

Figure 20. *Violin plots of the VV and TWI dimensions from LM2 input samples.*

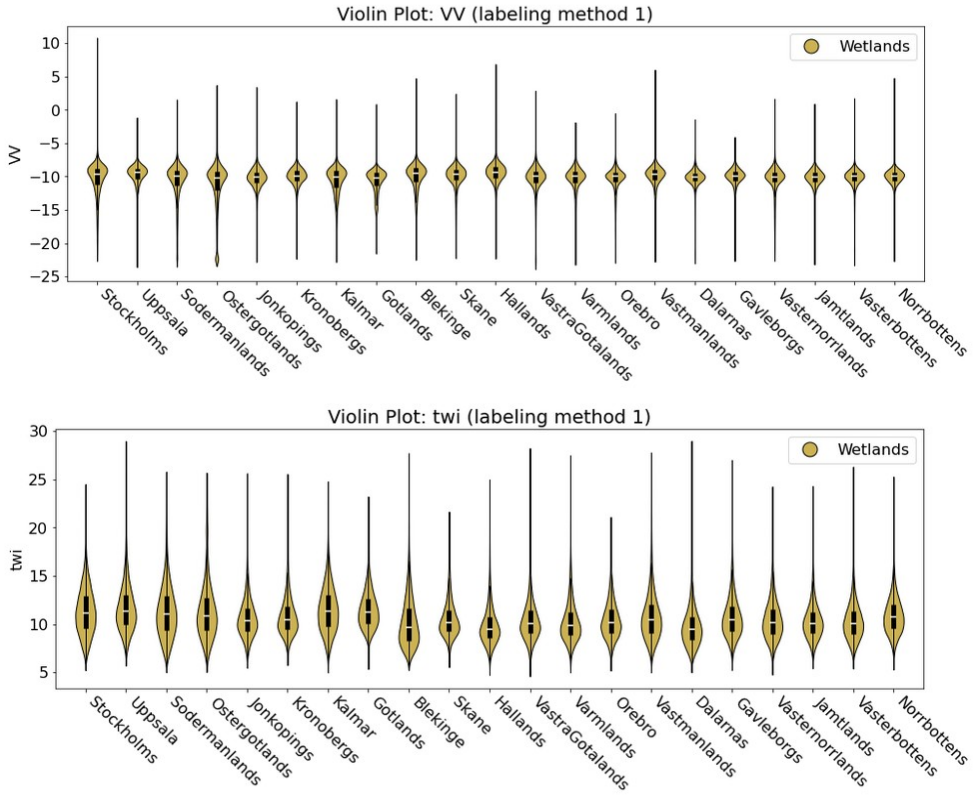

Figure 21. *Violin plots of the VV and TWI dimensions from LM1 input samples.*

The multi-temporal feature of the data was highly beneficial, specially for the inclusion of optical imagery, since it allows the preparation of cloudless inputs, with a reduced effect of shadows. It was apparent that the effect of shadows in the optical imagery was not completely accounted for, even with all the considerations taken in this regard. Thus, longer temporal ranges could be used in the future to overcome the traces of shadows in the input.

A recent study (Ståhl & Weimann, 2022) indicates that the historical wetlands area in Jönköping is 1,800 km^2, ~56% higher than what was surveyed in VMI, and 245% higher than what is found in RFWI. If agriculture is widespread in Jönköping, there is a great possibility that drainage, and destruction of wetlands happened in the last 20-30 years. The same study propagated the Jönköping model to most counties (excluding Jämtland, Västernorrland, Västerbotten and Norrbotten), predicting a wetland coverage of 19,600 km^2. They compare it to 7,820 km^2 calculated by the Swedish Mapping, Cadastral, and Land Registration Authority (Lantmäteriet). VMI in the region covers 14,487 km^2, while RFWI predictions estimate 15,889 km^2 of wetlands. Showing great differences in wetlands coverage between local sources.

RFWI has a very strong agreement with LUCAS, points classified in the first as wetlands and surveyed as non-wetlands in the second, are probably due to the overlap between reflectance signatures of vegetation like woodlands, shrublands, grasslands, and wetlands. Additionally, it should be noted that more than half (58.32%) of the 18,693 points belonging to these three classes, located in Sweden, were surveyed from an office. The definitions are not very clear, woodlands include areas covered by trees, of at least 10%. Shrublands include areas dominated by shrubs (at least 10% of the surface), and low-height plants. And some of the wetlands found in VMI have sparse vegetation distinguishable in Google Earth, creating uncertainty. On the other hand, many LUCAS wetland samples classified as non-wetlands in RFWI, are found close enough to RFWI wetlands to suggest that the extent of wetlands might have shrunk since 2018.

The area of wetlands according to ESA WorldCover, and MODIS LC1 products are much smaller than those of RFWI and VMI. Although ESA WorldCover underestimates wetlands' area, it was visually found to include many inland wetlands not found in MODIS (e.g. Fäjemyr). MODIS wetlands are only found in the interface between land and water LC, missing inland wetlands that are everywhere in Sweden, and explaining how MODIS over-appreciated the wetlands area in Stockholm (when compared to VMI), due to the county's lengthy coastline. ESA WorldCover differentiates herbaceous wetlands (class 90) from mangroves (class 95), and moss & lichen (class 100). It is known that moss and lichen can thrive in wetlands, e.g. Fäjemyr (Figure 10), nevertheless, the comparisons performed were only against herbaceous wetlands. There were no pixels classified as mangroves in Sweden, and Moss & Lichen class only existed in the northern counties (Dalarna, Gävleborg, Västernorrland, Jämtland, Västerbotten, and Norrbotten). The Ramsar Database includes many more wetlands than other global products, and many polygons are very well delineated, but it contains errors (Section 3.6). Ramsar's objectives might differ from mapping every wetland worldwide, nevertheless, it does not fully capture wetlands in Sweden.

At the same time, coastal wetlands in RFWI might be underestimated, because coastlines (from Lantmäteriet's Översiktskartan) were found in satellite imagery overlaying what is

unequivocally land. RFWI does not include some wetlands present in VMI that are outside the coastlines, due to VMI overlaying the coastlines in Lantmäteriet Översiktskartan.

It must be mentioned (regardless of the study's objectives for classifying wetlands), that water presented the highest user's, and producer's accuracies with both labeling methods. It can be seen how samples corresponding to water pixels (Figure 19) show different means, and distributions to those of wetlands, and non-wetlands, making water more easily separable.

5.3 Experience and issues with GEE

GEE computation timed out errors are the main reasons behind a single classifier being trained for each county. The stratified sampling algorithm consistently timed out when more than one county was selected to sample points from, and extents greater than 50,000 km^2 were observed to trigger errors.

The results obtained with GEE are reproducible, and the accuracies are close to constant. Variations are not greater than 1% when the stratified sampling algorithm's seed (in charge of randomizing the location of points) is changed.

Google Earth Engine platform's performance is remarkable, the ease of selecting, filtering, combining, and processing multi-temporal, and multi-source imagery gives researchers tools not available before. A huge asset for the academic community, since it is commercial use is possible not yet. Without the GEE platform, the realization of this study was not plausible due to temporal, and computational constraints of mapping the vast territory of Sweden.

The execution of the whole Google Earth Engine workflow for each county, from the very beginning up to the end of the training and validation steps (excluding the preparation of statistics) where the outputs are exported, is performed in a single run. Despite of the little time taken by GEE, not more than 5 minutes to train the classifier, even for the biggest county, and between 10-120 minutes to classify, and export the imagery of an entire county, depending on its size. It should be considered a limitation of the GEE environment that the separation of the workflow into smaller blocks was not an option, due to the impossibility of exporting assets (on the cloud inside the GEE platform) bigger than 300 GB. Thus, it is difficult to evaluate the results of inter-medium steps.

When working in GEE it is of fundamental importance to assess the computational requirements of each step. 'C*omputation timed out*', and '*user memory limit exceeded*' errors are common, specially when processing vast temporal and spatial extents. Not vital functions and algorithms must be discarded so that they do not allocate resources, and memory required by later steps. During this study, vectorial data polygons with complex geometries triggered these errors, when used to clip rasters or to limit point sampling within a region, even if their weight is negligible when compared to the rasterial data. It is generally a good practice to simplify such geometries or to employ simpler rectangular geometries whenever possible.

5.4 Recommendations for future studies

The uncertainties attached to the labels are the most likely cause of errors in this study, observed in the overestimation of wetland areas in Stockholm and Jämtland. VMI data was very reliable

in some counties, allowing easier identification, and digitization of wetland polygons for LM2 that was used for RFWI. Nonetheless, the identification of wetlands using Google Earth, and VMI polygons in the northern counties was a rather complex task. The satellite imagery in Jämtland, Västernorrland, Västerbotten, and Norrbotten is not fully curated as in other counties. Many of these counties' wetlands were covered by snow in Google Earth imagery. Ideally, the points used for training/validation would be hand-picked, but this is a very time-consuming, and repetitive task. Thus, better labeling can be achieved with more time and people involved.

LM2 was performed to overcome the uncertainties attached to LM1, more specifically, the chance of having a reference site with a wrong label, there is still uncertainty that might have propagated from VMI, and affected the results of using LM2 for classification (used for generating the new product RFWI in this study). Google Earth displays true color composites, mixing imagery from a wide range of sources, captured, and processed in different ways, and on different dates, some are from 2022, and some were captured in 2008. City centers are very curated, heavily processed, and have an outstanding spatial accuracy, while remote areas in Norrbotten, for example, can present very low spatial resolution, and errors in the imagery (Figure 22). Thus, because of the dynamic nature of wetlands, there is a chance that some of the polygons digitized inside VMI polygons, while looking at Google Earth satellite imagery, are areas without wetlands, ultimately causing misclassifications.

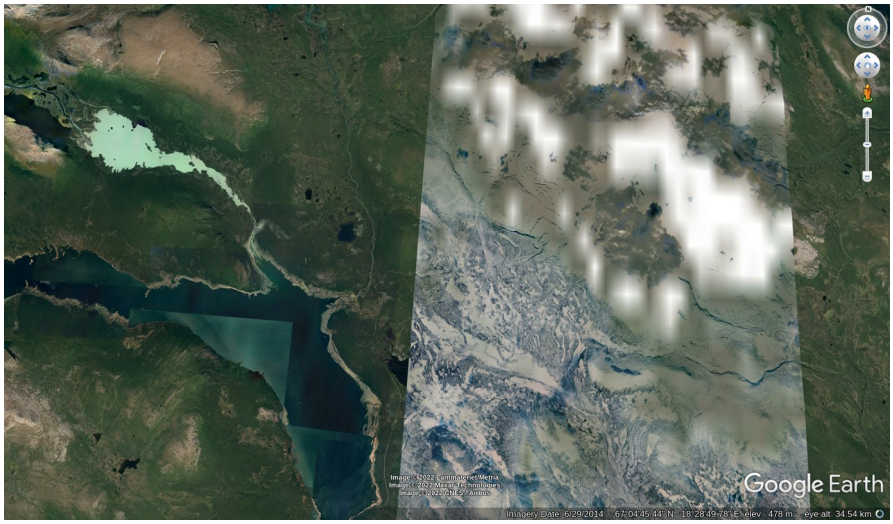

***Figure 22**. Google Earth screenshot, zoomed in Norrbotten.*

Figure 18 illustrates promising results from classifying topographical data with high spatial resolution (2 m), cutting more than half of probably misclassified wetland areas. Those results were achieved by classifying the higher spatial resolution with the same classifier trained with the coarser spatial resolution (50 m) topographical data, used for RFWI. It is recommended to use finer spatial resolution than 50 m in the future to at least match Sentinel's spatial resolution (10 m), for more accurate results. In despite that both datasets (50 m and 2 m) have the same minimum, maximum, and means, results might differ to those showed in this study, since the classifiers were trained with the 50 m data and the 2 m data was used only in the classification step.

Despite of LUCAS having a smaller amount of samples, the points are better spatially spread

than the polygons digitized for LM2. Thus, using LUCAS as ground truth data for labeling samples would suppose an interesting approach to consider in future studies. This has been already implemented in research focused on crop mapping (Shelestov et al., 2017)

There are multiple algorithms for calculating Slope, TPI and TWI, ranked the highest in the feature importance, similar to whatHird et al. (2017) previously suggested, expert knowledge should be used to assess the information derived from DEMs. NDVI, and NDWI ranked better than the bands from which they were derived, and thus, the inclusion of additional indices could be beneficial, e.g. Chen et al. (2017) did not include any data directly from satellite data bands but used satellite-derived indices (EVI, NDVI, LSWI, mNDWI).

Mahdianpari et al. (2019) used monthly composites with data from multiple years, i.e. compositing multi-temporal rasters from images captured during June, July, and August, over a 3 or 4-year period. This was not tested, and the reflectances of wetlands have been found to change even on a monthly basis, therefore, it would be appropriate to test more multi-temporal combinations for the preparation of inputs.

Mahdianpari et al. (2020) & Tian et al. (2016) stated the benefits of object-based feature selection (the equivalent of the labeled points sample implemented during the study) over pixel-wise classifications. The comparison of both approaches was not plausible during this study, and this could be interesting to test for Swedish wetlands. On the other hand, Zhao (2020) mapped mangroves, and compared the results between pixel-wise and object-oriented classifications, and finding that the pixel-wise technique performed better than the object-oriented.

The orthogonal transformation of Sentinel-2 optical data to a new multivariate space performed in PCA has been found to increase accuracies (Rana & Venkata Suryanarayana, 2020), and can be incorporated into the GEE workflow (Google, n.d.-c) in future studies to investigate if it can improve the accuracy of classifying wetlands.

6 Conclusions

Wetlands were mapped in Sweden, producing a new wetlands inventory (RFWI), using recent data and training a Random Forests classifier in each county. RFWI is comparable to VMI in many aspects, but captures finer scale details, and includes many smaller wetlands, it also captured wetlands that dissapeared since VMI was surveyed. The high accuracies of RFWI, and the agreement between RFWI, VMI, and LUCAS indicate that some steps were taken in the right direction for correctly mapping wetlands in Sweden. The combination of multi-source data with multi-temporal characteristics was fundamental for classifying wetlands with Random Forest. Nonetheless, the methods have limitations, and the accuracies of the validation set are over-optimistic due to spatial autocorrelation, and a very few amount of classes.

Differentiating between wetland types is the next step for the further development of an accurate national wetlands inventory. And the implementation of the workflow developed during this study can be used to generate land cover time-series, and monitor the time-wise evolution of wetlands in Sweden and other regions.

The areas classified as wetlands in RFWI must be closer to reality than those of VMI due to the addition of new smaller wetlands and details. Nevertheless, RFWI is not entirely reliable, areas with land covers different to wetlands are classified as such, and otherwise. Additionally, overestimations of the wetland coverage are very high in Jämtland, and Stockholm. Through the literature review of wetlands mapping performed in Sweden, it is concluded that the real wetlands area in Sweden must be within the range of VMI and RFWI. Existing large-scale products underestimate wetlands coverage in Sweden. Regardless of slight differences in the accepted definition of wetlands between authors, the areal coverage of wetlands in global, continental, and national maps, and inventories of Sweden differ greatly. Wetlands are dynamic, and diverse ecosystems that change at different rates, depending on multiple factors, this makes complex the task of mapping, and monitoring wetlands. Additionally, the spectral signatures of wetlands, and other vegetation, overlap in the latest imagery (Amani, Mahdavi, et al., 2019).

GEE played a huge role in the gathering of data, and training the random forest algorithm. There are methodologies, and algorithms not considered during this study, that can be taken to decrease uncertainties, and narrow the range of wetlands occurrence in Sweden (Section 5.4). The workflow of this study is reproducible, and the developed are scripts open-source, with the intention that further development can be done in this subject. Since the first step for the conservation of valuable ecosystems is their accurate identification.

References

Adam, E., Mutanga, O., & Rugege, D. (2010). Multispectral and hyperspectral remote sensing for identification and mapping of wetland vegetation: A review. *Wetlands Ecology and Management*, *18*(3), 281–296. https://doi.org/10.1007/s11273-009-9169-z

Amani, M., Brisco, B., Afshar, M., Mirmazloumi, S. M., Mahdavi, S., Mirzadeh, S. M. J., Huang, W., & Granger, J. (2019). A generalized supervised classification scheme to produce provincial wetland inventory maps: An application of Google Earth Engine for big geo data processing. *Big Earth Data*, *3*(4), 378–394. https://doi.org/10.1080/20964471.2019.1690404

Amani, M., Mahdavi, S., Afshar, M., Brisco, B., Huang, W., Mohammad Javad Mirzadeh, S., White, L., Banks, S., Montgomery, J., & Hopkinson, C. (2019). Canadian Wetland Inventory using Google Earth Engine: The First Map and Preliminary Results. *Remote Sensing*, *11*(7), 842. https://doi.org/10.3390/rs11070842

Amoakoh, A. O., Aplin, P., Awuah, K. T., Delgado-Fernandez, I., Moses, C., Alonso, C. P., Kankam, S., & Mensah, J. C. (2021). Testing the Contribution of Multi-Source Remote Sensing Features for Random Forest Classification of the Greater Amanzule Tropical Peatland. *Sensors*, *21*(10), 3399. https://doi.org/10.3390/s21103399

Ballin, M., Barcaroli, G., Masselli, M., & Scarnó, M. (2018). *Redesign sample for Land Use/Cover Area frame Survey (LUCAS) 2018*. Statistical Office of the European Union. European Commission. https://data.europa.eu/doi/10.2785/132365

Basham May, A. M., Pinder, J. E., & Kroh, G. C. (1997). A comparison of Landsat Thematic Mapper and SPOT multi-spectral imagery for the classification of shrub and meadow vegetation in northern California, U.S.A. *International Journal of Remote Sensing*, *18*(18), 3719–3728. https://doi.org/10.1080/014311697216577

Batzer, D., & Sharitz, R. (2007). Ecology of Freshwater and Estuarine Wetlands. *Ecology of Freshwater and Estuarine Wetlands*. https://doi.org/10.1525/california/9780520247772.003.0001

Beck, H. E., Zimmermann, N. E., McVicar, T. R., Vergopolan, N., Berg, A., & Wood, E. F. (2018). Present and future Köppen-Geiger climate classification maps at 1-km resolution. *Scientific Data*, *5*(1), 180214. https://doi.org/10.1038/sdata.2018.214

Berhane, T., Lane, C., Wu, Q., Autrey, B., Anenkhonov, O., Chepinoga, V., & Liu, H. (2018). Decision-Tree, Rule-Based, and Random Forest Classification of High-Resolution Multispectral Imagery for Wetland Mapping and Inventory. *Remote Sensing*, *10*(4), 580. https://doi.org/10.3390/rs10040580

Breiman, L. (2001). Random forests. *Machine Learning*, *45*(1), 5–32. Scopus. https://doi.org/10.1023/A:1010933404324

Chen, B., Xiao, X., Li, X., Pan, L., Doughty, R., Ma, J., Dong, J., Qin, Y., Zhao, B., Wu, Z., Sun, R., Lan, G., Xie, G., Clinton, N., & Giri, C. (2017). A mangrove forest map of China in 2015: Analysis of time series Landsat 7/8 and Sentinel-1A imagery in Google Earth Engine cloud computing platform. *ISPRS Journal of Photogrammetry and Remote Sensing*, *131*, 104–120. https://doi.org/10.1016/j.isprsjprs.2017.07.011

Chuvieco, E. (2016). Fundamentals of satellite remote sensing: An environmental approach. *International Journal of Digital Earth*, *9*(12), 1275–1276. https://doi.org/10.1080/17538947.2016.1209938

Corcoran, J. M. (2013). *Influence of Multi-Source and Multi-Temporal Remotely Sensed and Ancillary Data on the Accuracy of Random Forest Classification of Wetlands in Northern Minnesota*. 27.

Costanza, R., d'Arge, R., de Groot, R., Farber, S., Grasso, M., Hannon, B., Limburg, K., Naeem,

S., O'Neill, R. V., Paruelo, J., Raskin, R. G., Sutton, P., & van den Belt, M. (1997). The value of the world's ecosystem services and natural capital. *Nature*, *387*(6630), 253–260. https://doi.org/10.1038/387253a0

Dang, K. B., Nguyen, M. H., Nguyen, D. A., Phan, T. T. H., Giang, T. L., Pham, H. H., Nguyen, T. N., Tran, T. T. V., & Bui, D. T. (2020). Coastal Wetland Classification with Deep U-Net Convolutional Networks and Sentinel-2 Imagery: A Case Study at the Tien Yen Estuary of Vietnam. *Remote Sensing*, *12*(19), 3270. https://doi.org/10.3390/rs12193270

Davidson. (2014). How much wetland has the world lost? Long-term and recent trends in global wetland area. *Marine and Freshwater Research*, *65*(10), 934. https://doi.org/10.1071/MF14173

Davidson, E. A., & Janssens, I. A. (2006). Temperature sensitivity of soil carbon decomposition and feedbacks to climate change. *Nature*, *440*(7081), 165–173. https://doi.org/10.1038/nature04514

Erwin, K. L. (2009). Wetlands and global climate change: The role of wetland restoration in a changing world. *Wetlands Ecology and Management*, *17*(1), 71–84. https://doi.org/10.1007/s11273-008-9119-1

ESA. (2020). *WorldCover Product User Manual*. https://worldcover2020.esa.int/data/docs/WorldCover_PUM_V1.1.pdf

ESA. (2021). *WorldCover Product Validation Report*. https://worldcover2020.esa.int/data/docs/WorldCover_PVR_V1.1.pdf

European Space Agency. (n.d.-a). *Sentinel-1- Observation Scenario—Planned Acquisitions—Sentinel Online*. Retrieved March 26, 2022, from https://sentinels.copernicus.eu/web/sentinel/missions/sentinel-1/observation-scenario

European Space Agency. (n.d.-b). *Sentinel-1—Instrument Payload—Sentinel Online—Sentinel Online*. Retrieved March 22, 2022, from https://sentinel.esa.int/web/sentinel/missions/sentinel-1/instrument-payload

European Space Agency. (2015). *Sentinel-2 User Handbook*. *1*, 64.

Finlayson, C. (1995). *Wetland Classification and Inventory: A Summary*. 9.

Friedl, M. A., Gopal, S., Muchoney, D., & Strahler, A. H. (2000). Global land cover mapping from MODIS: Algorithm design and preliminary results. *IGARSS 2000. IEEE 2000 International Geoscience and Remote Sensing Symposium. Taking the Pulse of the Planet: The Role of Remote Sensing in Managing the Environment. Proceedings (Cat. No.00CH37120)*, *2*, 527–529. https://doi.org/10.1109/IGARSS.2000.861618

Friedl, M. A., Sulla-Menashe, D., Tan, B., Schneider, A., Ramankutty, N., Sibley, A., & Huang, X. (2010). MODIS Collection 5 global land cover: Algorithm refinements and characterization of new datasets. *Remote Sensing of Environment*, *114*(1), 168–182. https://doi.org/10.1016/j.rse.2009.08.016

Géron, A. (2019). *Hands-On Machine Learning with Scikit-Learn, Keras, and TensorFlow*.

Ghorbanian, A., Zaghian, S., Asiyabi, R. M., Amani, M., Mohammadzadeh, A., & Jamali, S. (2021). Mangrove Ecosystem Mapping Using Sentinel-1 and Sentinel-2 Satellite Images and Random Forest Algorithm in Google Earth Engine. *Remote Sensing*, *13*(13), 2565. https://doi.org/10.3390/rs13132565

Google. (n.d.-a). *Earth Engine Code Editor*. Retrieved May 10, 2022, from https://code.earthengine.google.com/

Google. (n.d.-b). *Ee.Classifier.smileRandomForest | Google Earth Engine*. Google Developers. Retrieved April 8, 2022, from https://developers.google.com/earth-engine/apidocs/ee-classifier-smilerandomforest

Google. (n.d.-c). *Eigen Analysis | Google Earth Engine*. Google Developers. Retrieved May 9, 2022, from https://developers.google.com/earth-engine/guides/arrays_eigen_analysis

Google. (n.d.-d). *Sentinel-1 SAR GRD: C-band Synthetic Aperture Radar Ground Range Detected, log scaling | Earth Engine Data Catalog | Google Developers*. Retrieved April 3, 2022, from https://developers.google.com/earth-engine/datasets/catalog/COPERNICUS_S1_GRD

Google. (n.d.-e). *Sentinel-2 MSI: MultiSpectral Instrument, Level-2A | Earth Engine Data Catalog | Google Developers*. Retrieved May 5, 2022, from https://developers.google.com/earth-engine/datasets/catalog/COPERNICUS_S2_SR

Gorelick, N., Hancher, M., Dixon, M., Ilyushchenko, S., Thau, D., & Moore, R. (2017). Google Earth Engine: Planetary-scale geospatial analysis for everyone. *Remote Sensing of Environment*, *202*, 18–27. https://doi.org/10.1016/j.rse.2017.06.031

Gunnarsson, U., & Löfroth, M. (2009). *Våtmarksinventeringen: Resultat från 25 års inventeringar ; nationell slutrapport för våtmarksinventeringen (VMI) i Sverige*. Naturvårdsverket.

Gunnarsson, U., Löfroth, M., Sandring, S., & Gunnarsson, U. (2014). *The Swedish wetland survey: Compiled excerpts from the national final report*. Swedish Environmental Protection Agency.

Hird, J. N., DeLancey, E. R., McDermid, G. J., & Kariyeva, J. (2017). *Google Earth Engine, Open-Access Satellite Data, and Machine Learning in Support of Large-Area Probabilistic Wetland Mapping*. 27.

Howland, W. G. (1980). MuItispectraI Aerial Photography for Wetland Vegetation Mapping. *PHOTOGRAMMETRIC ENGINEERING*, 13.

Huang, C., Davis, L. S., & Townshend, J. R. G. (2002). An assessment of support vector machines for land cover classification. *International Journal of Remote Sensing*, *23*(4), 725–749. https://doi.org/10.1080/01431160110040323

Huete, A., Didan, K., Miura, T., Rodriguez, E. P., Gao, X., & Ferreira, L. G. (2002). Overview of the radiometric and biophysical performance of the MODIS vegetation indices. *Remote Sensing of Environment*, *83*(1–2), 195–213. https://doi.org/10.1016/S0034-4257(02)00096-2

Keane, J. B., Toet, S., Ineson, P., Weslien, P., Stockdale, J. E., & Klemedtsson, L. (2021). Carbon Dioxide and Methane Flux Response and Recovery From Drought in a Hemiboreal Ombrotrophic Fen. *Frontiers in Earth Science*, *8*, 13.

Lamb, B. T., Tzortziou, M. A., & McDonald, K. C. (2019). Evaluation of Approaches for Mapping Tidal Wetlands of the Chesapeake and Delaware Bays. *Remote Sensing*, *11*(20), 2366. https://doi.org/10.3390/rs11202366

Länsstyrelsen Skåne. (2016). *Bevarandeplan för Natura 2000-området Fäjemyr SE0420290*.

Lantmäteriet. (n.d.-a). *Markhöjdmodell Nedladdning, grid 1+*. Lantmateriet.se. Retrieved May 9, 2022, from https://www.lantmateriet.se/sv/Kartor-och-geografisk-information/geodataprodukter/produktlista/markhojdmodell-nedladdning-grid-1/

Lantmäteriet. (n.d.-b). *Markhöjdmodell Nedladdning, grid 50+*. Lantmateriet.se. Retrieved May 9, 2022, from https://www.lantmateriet.se/sv/Kartor-och-geografisk-information/geodataprodukter/produktlista/markhojdmodell-nedladdning-grid-50/

Lantmäteriet. (n.d.-c). *Översiktskartan*. Lantmateriet.se. Retrieved April 4, 2022, from https://www.lantmateriet.se/sv/Kartor-och-geografisk-information/geodataprodukter/produktlista/oversiktskartan/

Lantmäteriet. (2019). *National DEM Quality Description*. https://www.lantmateriet.se/globalassets/kartor-och-geografisk-information/hojddata/quality_description_dem.pdf

Lantmäteriet. (2021). *GSD-Elevation data, grid 50+ nh*. https://www.lantmateriet.se/globalassets/kartor-och-geografisk-information/hojddata/e_grid50plus_nh.pdf

Lehner, B., & Döll, P. (2004). Development and validation of a global database of lakes, reservoirs and wetlands. *Journal of Hydrology*, *296*(1–4), 1–22. https://doi.org/10.1016/j.jhydrol.2004.03.028

Mahdianpari, M., Salehi, B., Mohammadimanesh, F., Brisco, B., Homayouni, S., Gill, E., DeLancey, E. R., & Bourgeau-Chavez, L. (2020). Big Data for a Big Country: The First Generation of Canadian Wetland Inventory Map at a Spatial Resolution of 10-m Using Sentinel-1 and Sentinel-2 Data on the Google Earth Engine Cloud Computing Platform. *Canadian Journal of Remote Sensing*, *46*(1), 15–33. https://doi.org/10.1080/07038992.2019.1711366

Mahdianpari, M., Salehi, B., Mohammadimanesh, F., Homayouni, S., & Gill, E. (2019). The First Wetland Inventory Map of Newfoundland at a Spatial Resolution of 10 m Using Sentinel-1 and Sentinel-2 Data on the Google Earth Engine Cloud Computing Platform. *Remote Sensing*, *11*(1), 43. https://doi.org/10.3390/rs11010043

McCarthy, J., Gumbricht, T., & McCarthy, T. S. (2005). Ecoregion classification in the Okavango Delta, Botswana from multitemporal remote sensing. *International Journal of Remote Sensing*, *26*(19), 4339–4357. https://doi.org/10.1080/01431160500113583

Mitsch, W. J., Bernal, B., Nahlik, A. M., Mander, Ü., Zhang, L., Anderson, C. J., Jørgensen, S. E., & Brix, H. (2013). Wetlands, carbon, and climate change. *Landscape Ecology*, *28*(4), 583–597. https://doi.org/10.1007/s10980-012-9758-8

Naturvårdsverket. (n.d.). *VMI [Data set]*. Retrieved April 6, 2022, from http://miljodataportalen.naturvardsverket.se

OSGEO. (n.d.). *gdaldem—GDAL documentation*. Retrieved April 4, 2022, from https://gdal.org/programs/gdaldem.html

OSGEO. (2022). *r.watershed—GRASS GIS manual*. https://grass.osgeo.org/grass80/manuals/r.watershed.html

Ozesmi, S. L., & Bauer, M. E. (2002). Satellite remote sensing of wetlands. *Wetlands Ecology and Management*, *10*(5), 381–402. https://doi.org/10.1023/A:1020908432489

Ploton, P., Mortier, F., Réjou-Méchain, M., Barbier, N., Picard, N., Rossi, V., Dormann, C., Cornu, G., Viennois, G., Bayol, N., Lyapustin, A., Gourlet-Fleury, S., & Pélissier, R. (2020). Spatial validation reveals poor predictive performance of large-scale ecological mapping models. *Nature Communications*, *11*(1), 4540. https://doi.org/10.1038/s41467-020-18321-y

Podest, E., & McCartney, S. (2019). SAR for Flood Mapping using Google Earth Engine. *Applied Remote Sensing Training Program (ARSET) - Jet Propultion Lab (JPL) - National Aeronautics and Space Administration (NASA)*, 52.

Ramsar Convention Secretariat. (2016). *An Introduction to the Convention on Wetlands*. https://abs.igc.by/wp-content/uploads/2016/04/Introduction-to-the-Convention-on-Wetlands.-Ramsar-Handbooks-5th-Edition-2016.pdf

Rana, V. K., & Venkata Suryanarayana, T. M. (2020). Performance evaluation of MLE, RF and SVM classification algorithms for watershed scale land use/land cover mapping using sentinel 2 bands. *Remote Sensing Applications: Society and Environment*, *19*, 100351. https://doi.org/10.1016/j.rsase.2020.100351

Reddy, K. R., & DeLaune, R. D. (2008). *Biogeochemistry of wetlands: Science and applications*. CRC Press.

Shelestov, A., Lavreniuk, M., Kussul, N., Novikov, A., & Skakun, S. (2017). Exploring Google Earth Engine Platform for Big Data Processing: Classification of Multi-Temporal

Satellite Imagery for Crop Mapping. *Frontiers in Earth Science*, *5*. https://doi.org/10.3389/feart.2017.00017

Shima, L. J., Anderson, R. R., & Carter, V. P. (1976). The Use of Aerial Color Infrared Photography in Mapping the Vegetation of a Freshwater Marsh. *Chesapeake Science*, *17*(2), 74. https://doi.org/10.2307/1351049

Söderqvist, T. (2002). Constructed wetlands as nitrogen sinks in southern Sweden: An empirical analysis of cost determinants. *Ecological Engineering*, *19*(2), 161–173. https://doi.org/10.1016/S0925-8574(02)00039-3

Ståhl, N., & Weimann, L. (2022). Identifying wetland areas in historical maps using deep convolutional neural networks. *Ecological Informatics*, *68*, 101557. https://doi.org/10.1016/j.ecoinf.2022.101557

Teluguntla, P., Thenkabail, P. S., Oliphant, A., Xiong, J., Gumma, M. K., Congalton, R. G., Yadav, K., & Huete, A. (2018). A 30-m landsat-derived cropland extent product of Australia and China using random forest machine learning algorithm on Google Earth Engine cloud computing platform. *ISPRS Journal of Photogrammetry and Remote Sensing*, *144*, 325–340. https://doi.org/10.1016/j.isprsjprs.2018.07.017

Tian, S., Zhang, X., Tian, J., & Sun, Q. (2016). Random Forest Classification of Wetland Landcovers from Multi-Sensor Data in the Arid Region of Xinjiang, China. *Remote Sensing*, *8*(11), 954. https://doi.org/10.3390/rs8110954

Wu, Q., Lane, C. R., Li, X., Zhao, K., Zhou, Y., Clinton, N., DeVries, B., Golden, H. E., & Lang, M. W. (2019). Integrating LiDAR data and multi-temporal aerial imagery to map wetland inundation dynamics using Google Earth Engine. *Remote Sensing of Environment*, *228*, 1–13. https://doi.org/10.1016/j.rse.2019.04.015

Yun-gang, C., Li-juan, Y., & Ze-zhong, Z. (2008). *EXTRACTION OF INFORMATION ON GEOLOGY HAZARD FROM MULTI-POLARIZATION SAR IMAGES*. 4.

Zanaga, D., Van De Kerchove, R., De Keersmaecker, W., Souverijns, N., Brockmann, C., Quast, R., Wevers, J., Grosu, A., Paccini, A., Vergnaud, S., Cartus, O., Santoro, M., Fritz, S., Georgieva, I., Lesiv, M., Carter, S., Herold, M., Li, L., Tsendbazar, N.-E., … Arino, O. (2021). *ESA WorldCover 10 m 2020 v100* [Data set]. Zenodo. https://doi.org/10.5281/zenodo.5571936

Zedler, J. B., & Kercher, S. (2005). WETLAND RESOURCES: Status, Trends, Ecosystem Services, and Restorability. *Annual Review of Environment and Resources*, *30*(1), 39–74. https://doi.org/10.1146/annurev.energy.30.050504.144248

Zhao, C. (2020). 10-m-resolution mangrove maps of China derived from multi-source and multi-temporal satellite observations. *ISPRS Journal of Photogrammetry and Remote Sensing*, 17.

Appendix A: Additional figures

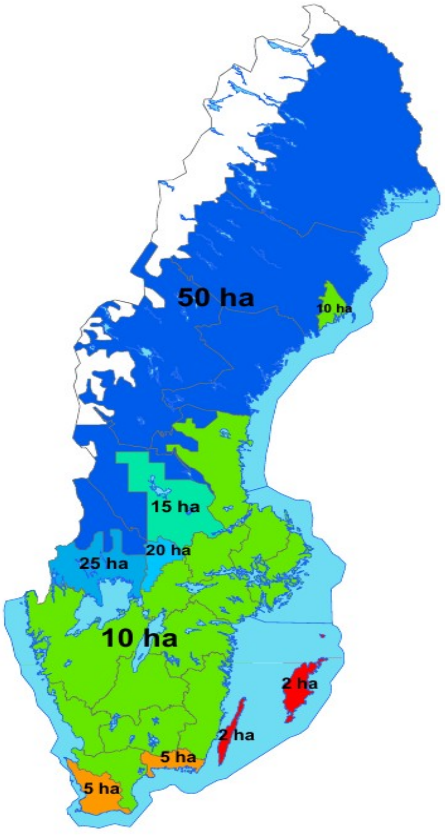

***Figure A.1**. Smallest wetlands in VMI (Gunnarsson & Löfroth, 2009).*

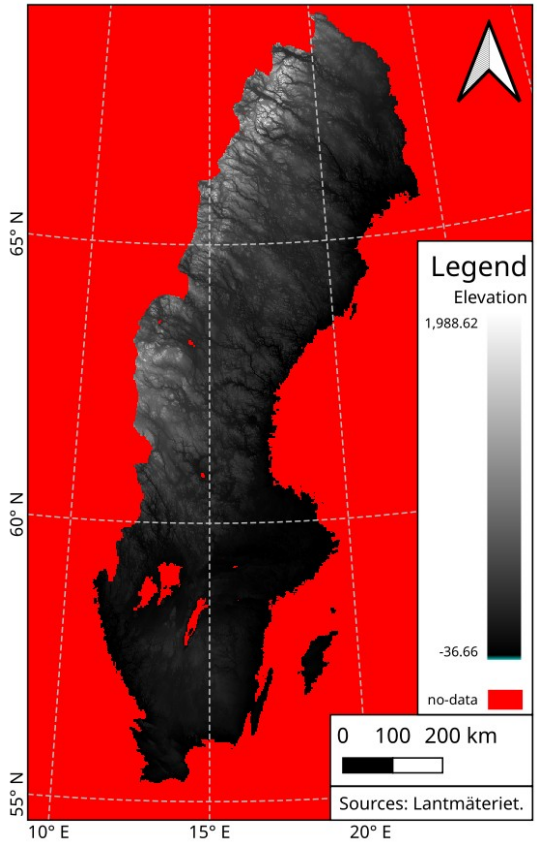

***Figure A.2**. Lantmäteriet's Grid 50+ GSD-elevation 2020 product (Based on data from).*

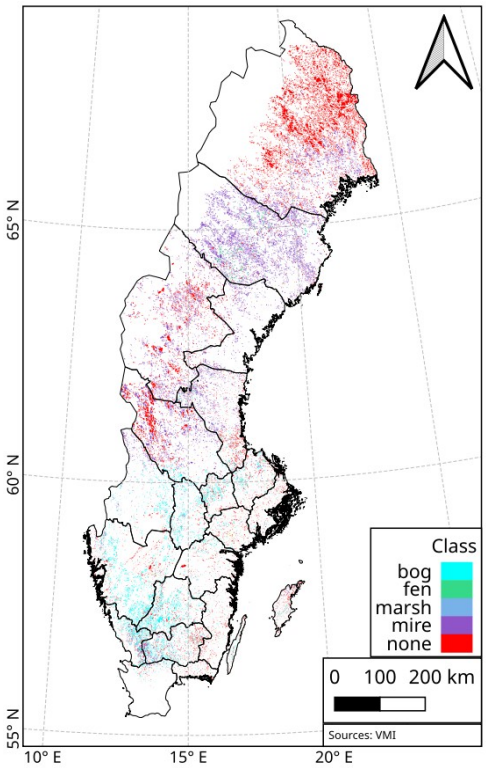

Figure A.4. *VMI wetland types (Based on data from).*

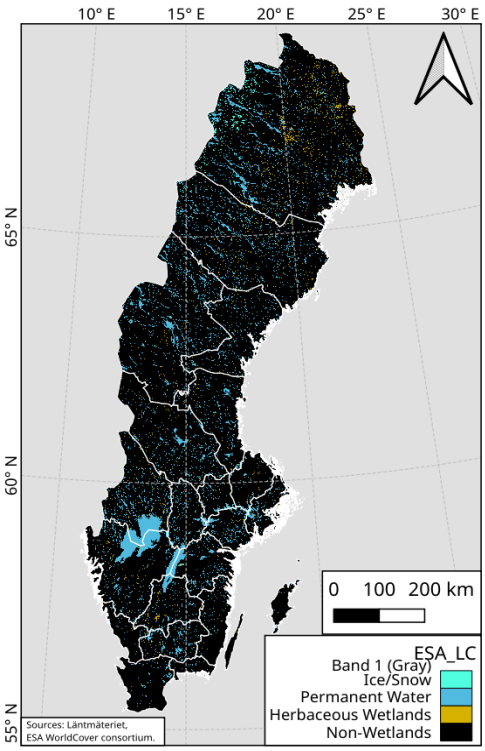

Figure A.3. *ESA WorldCover LC Product (Based on data from).*

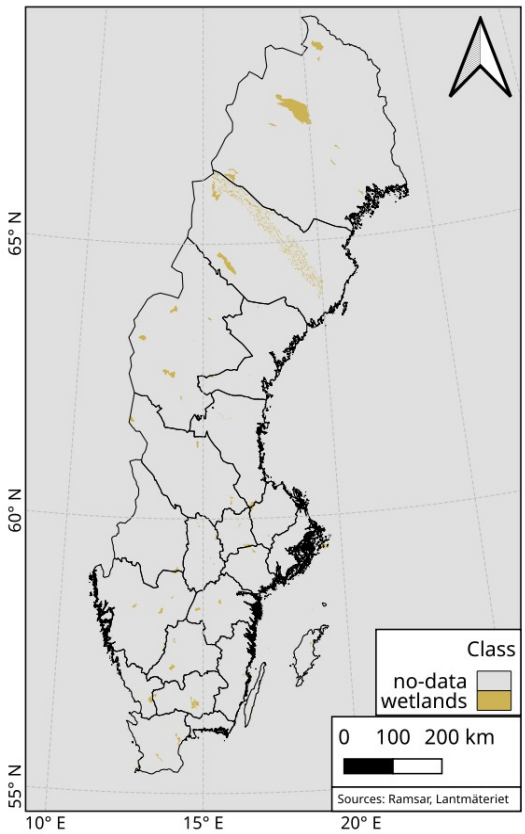

Figure A.5. *Ramsar Wetlands Database (Based on data from).*

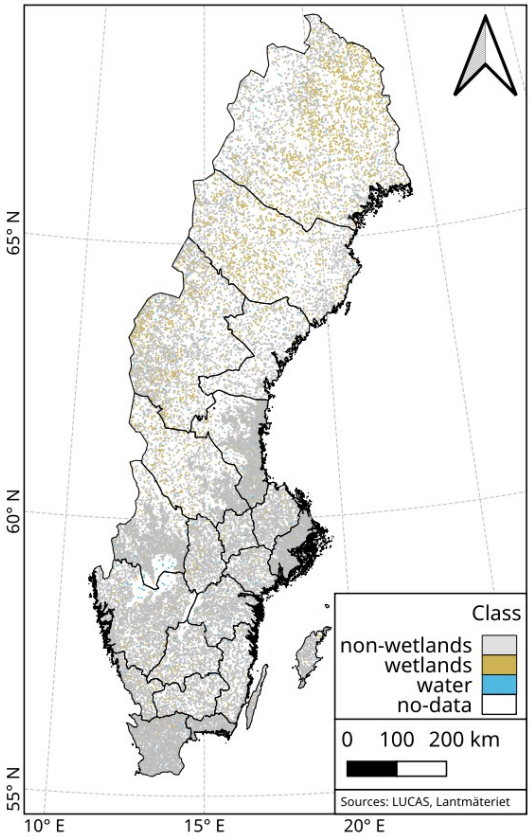

Figure A.6. LUCAS Dataset (Based on data from).

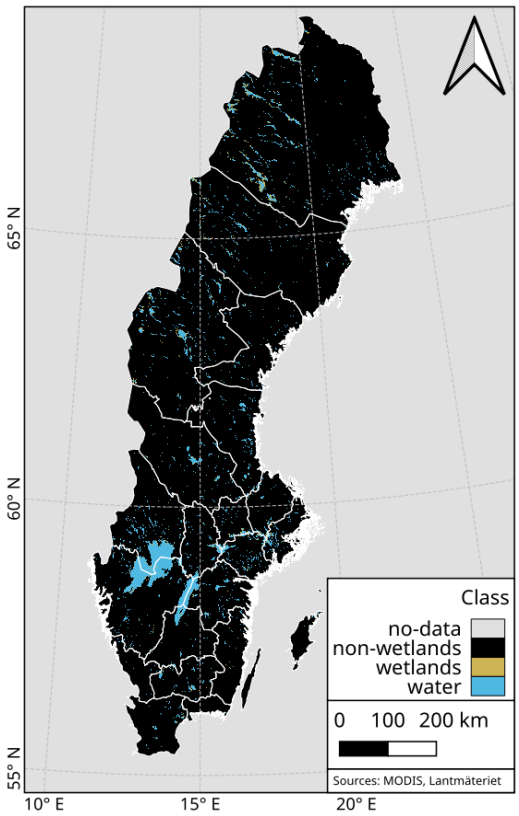

Figure A.7. MODIS LC1 Dataset (Based on data from).

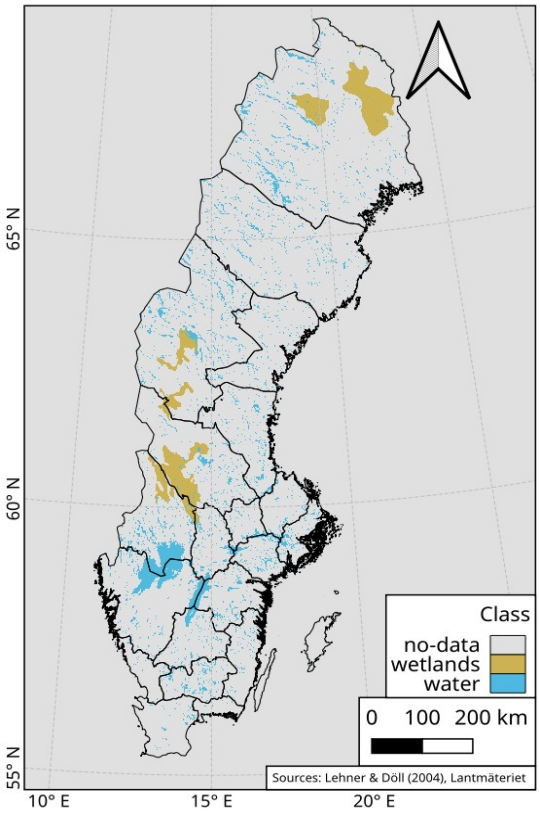

Figure A.8. *GLWD-3, Based on data from* Lehner & Döll (2004).

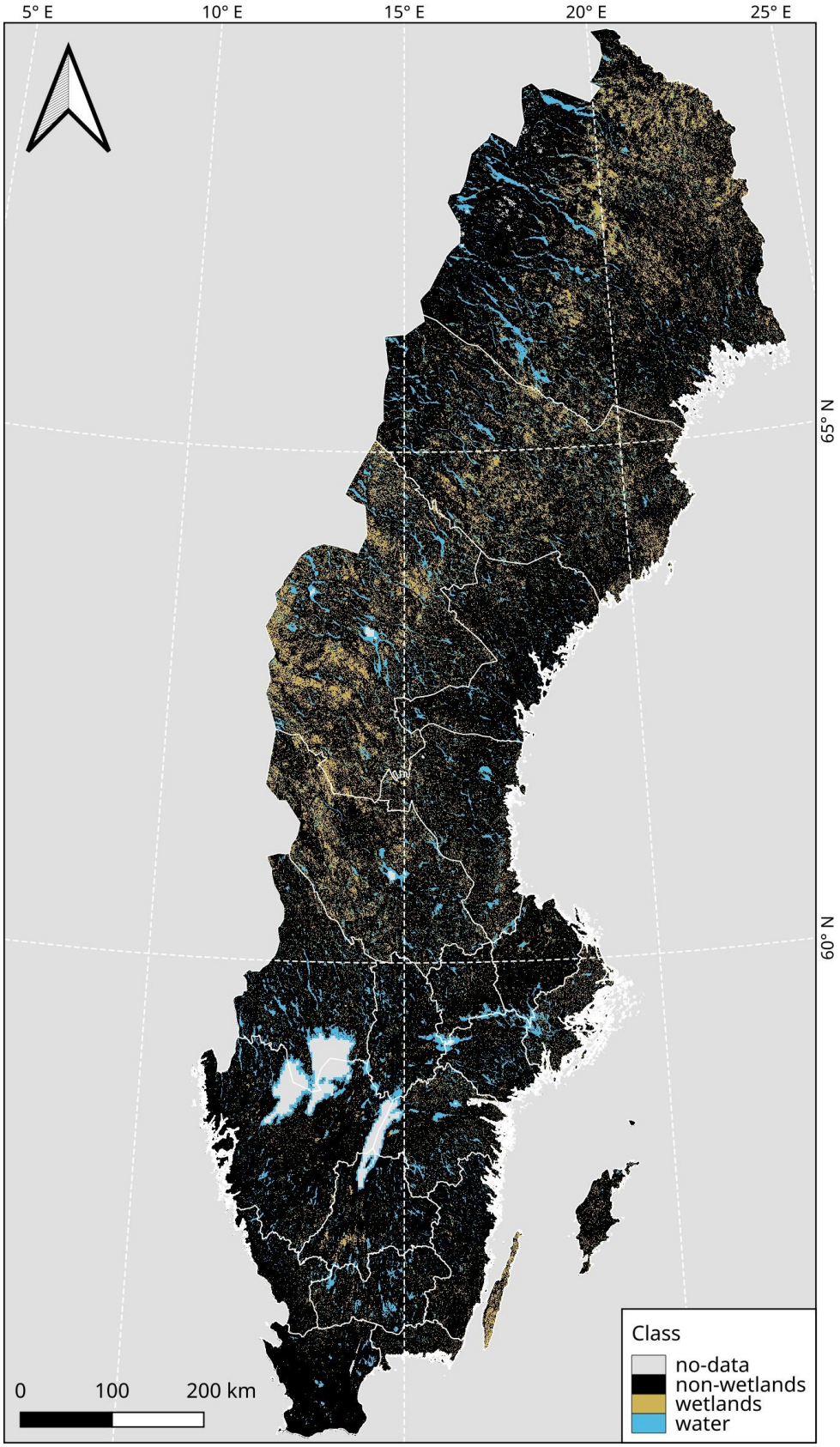

***Figure A.9**. RFWI (own).*

Appendix B: Additional tables

Table B.1. The accuracies and kappa coefficients of LM2's points validation set, per county.

Table B.2. The accuracies and kappa coefficients of LM1's points validation set, per county.

Table B.1. *RFWI classification accuracies county-wise, from using the labeling method 2 (LM2). Note: Producer's & User's are class-wise averages.*

	Training				Validation			
County	**Overall**	**Producer's**	**User's**	**Kappa**	**Overall**	**Producer's**	**User's**	**Kappa**
Stockholm	99.95	99.95	99.95	0.9992	99.34	99.34	99.34	0.9900
Uppsala	99.97	99.97	99.97	0.9995	98.96	98.96	98.96	0.9844
Södermanland	99.99	99.99	99.99	0.9998	99.67	99.67	99.67	0.9951
Östergötland	99.98	99.98	99.98	0.9998	99.57	99.57	99.57	0.9936
Jönköping	99.98	99.98	99.98	0.9997	99.29	99.29	99.29	0.9894
Kronoberg	99.99	99.99	99.99	0.9999	99.84	99.84	99.84	0.9976
Kalmar	99.93	99.93	99.93	0.9989	97.68	97.67	97.67	0.9652
Gotland	99.97	99.97	99.97	0.9996	99.28	99.28	99.28	0.9891
Blekinge	99.95	99.95	99.95	0.9993	98.82	98.82	98.82	0.9822
Skåne	99.94	99.94	99.94	0.9991	99.12	99.12	99.12	0.9868
Halland	99.96	99.96	99.96	0.9994	98.69	98.69	98.69	0.9804
Västra Götaland	99.99	99.99	99.99	0.9998	99.70	99.70	99.70	0.9956
Värmland	99.99	99.99	99.99	0.9998	99.70	99.70	99.70	0.9955
Örebro	99.92	99.92	99.92	0.9989	98.13	98.12	98.12	0.9719
Västmanland	99.96	99.96	99.96	0.9995	99.01	99.01	99.02	0.9851
Dalarna	99.95	99.95	99.95	0.9992	99.18	99.18	99.18	0.9878
Gävleborg	99.97	99.97	99.97	0.9995	99.12	99.12	99.12	0.9868
Västernorrland	99.91	99.91	99.91	0.9986	97.89	97.90	97.91	0.9684
Jämtland	99.93	99.93	99.93	0.9989	98.64	98.64	98.64	0.9797
Västerbotten	99.98	99.98	99.98	0.9997	99.44	99.44	99.44	0.9916
Norrbotten	99.93	99.93	99.93	0.9990	97.40	97.40	97.40	0.9610
Sweden	**99.96**	**99.96**	**99.96**	**0.9994**	**98.97**	**98.97**	**98.98**	**0.9846**

Table B.2. *Classification county-wise accuracies, from using the labeling method 1 (LM1). Note: Producer's & User's are class-wise averages.*

	Training				Validation			
County	Overall	Producers	User's	Kappa	Overall	Producers	User's	Kappa
Stockholm	99.42	99.42	99.42	0.9913	82.19	82.17	82.06	0.7328
Uppsala	99.42	99.42	99.42	0.9913	81.66	81.64	81.69	0.7250
Södermanland	99.37	99.37	99.37	0.9906	81.33	81.22	81.05	0.7198
Östergötland	99.35	99.35	99.35	0.9902	83.42	83.42	83.52	0.7513
Jönköping	99.40	99.40	99.40	0.9910	80.98	80.95	81.03	0.7146
Kronoberg	99.44	99.41	99.44	0.9916	82.72	82.14	82.23	0.7401
Kalmar	99.29	99.29	99.29	0.9894	85.20	85.22	85.11	0.7780
Gotland	99.52	99.48	99.63	0.9911	75.21	78.42	80.79	0.5355
Blekinge	99.39	99.39	99.40	0.9909	81.55	81.53	81.52	0.7233
Skåne	99.28	99.28	99.28	0.9892	82.56	82.61	82.46	0.7384
Halland	99.32	99.32	99.32	0.9898	78.44	78.46	78.32	0.6766
Västra Götaland	99.39	99.39	99.39	0.9908	82.10	82.08	81.93	0.7315
Värmland	99.43	99.43	99.44	0.9915	83.54	83.53	83.48	0.7531
Örebro	99.44	99.42	99.44	0.9906	71.22	71.45	72.24	0.5090
Västmanland	99.35	99.35	99.35	0.9902	84.58	84.58	84.47	0.7688
Dalarna	99.29	99.34	99.31	0.9893	81.46	82.81	82.42	0.7182
Gävleborg	99.34	99.27	99.33	0.9900	87.64	86.52	86.74	0.8116
Västernorrland	99.40	99.40	99.40	0.9910	84.82	84.78	84.70	0.7723
Jämtland	99.39	99.39	99.39	0.9908	83.80	83.84	83.80	0.7570
Västerbotten	99.32	99.32	99.32	0.9898	83.40	83.37	83.27	0.7510
Norrbotten	99.34	99.34	99.34	0.9901	84.19	84.22	84.16	0.7628
Sweden	**99.38**	**99.37**	**99.38**	**0.9905**	**82.00**	**82.14**	**82.24**	**0.7224**